Oblique rifting triggered by slab tearing : the case of the Alboran rifted margin in the eastern Betics

Marine Larrey[1,2], Frédéric Mouthereau[1*], Damien Do Couto[3], Emmanuel Masini[4], Anthony Jourdon[5], Sylvain Calassou[2] and Véronique Miegebielle[2]

[1]Université Paul Sabatier, Géosciences Environnement Toulouse, GET UMR 5563, Toulouse, France.

[2]TOTAL S.A., Centre Scientifique & Technique Jean Féger, Pau, France.

[3]Sorbonne Université, CNRS-INSU, Institut des Sciences de la Terre Paris, ISTeP UMR 7193, F-75005 Paris, France.

[4]M&U sas, France.

[5]Institute of Geophysics, Ludwig-Maximilians-Universität München, Munich, Germany.

Corresponding author: Frédéric Mouthereau (frederic.mouthereau@get.omp.eu)

Abstract

The tectonic evolution of highly oblique continental margins that result from extension above lithospheric STEP faults is poorly understood. Here, we investigate the case of the Alboran margin in the eastern Betics characterized by crustal thinning of 15-10 km, oblique to the direction of slab retreat. The current deformation patterns indicate that oblique rifting is underway. However, it is unclear whether these conditions are those that prevailed during the formation of the metamorphic domes and intramontane basins. We review the temporal and spatial evolution of Neogene sedimentary basins and brittle deformation in the eastern Betics, and exploit offshore seismic reflection lines to propose a crustal-scale section across the oblique margin. The history of sediment infill and rates of subsidence combined with the analyses of fault slip data, confirm that brittle extension oriented from N20°E to EW occurred during an interval spanning from the Serravallian-early Tortonian to the late Tortonian (14-8 Ma). This extension is associated with both normal and strike-slip regimes and the evolution of the strike-slip fault zones flanking the metamorphic domes. The transtensional model forms a coherent scheme linking the ductile deformation associated with metamorphic domes and the formation of EW- and NW-SE/NNW-SSE-directed sedimentary basins in the brittle upper crust during the Tortonian. The oblique extension, which is closely associated with STEP faulting, occurred during the regional convergence between Africa and Iberia since the Miocene. Only recently, around 8 Ma, slab detachment started to migrate westward, leading to tectonic inversion in the eastern Betics. Such a type of narrow oblique rifted margin associated with transform-like plate boundaries is not unique but is expected to be hardly preserved in the geological record due to the transient nature of retreating subduction systems.

1 Introduction

1.1 Tear faulting and oblique crustal thinning in the Betics

Lithospheric tear faults or subduction-transform edge propagator (STEP) faults are propagating strike-slip faults that accommodate the differential motion between the retreating subduction zone and the overriding plate (Govers and Wortel, 2005). Because of the relative motion between back-arc and surrounding plates, they are also propagating strike-slip faults defined by a sharp contrast in crustal thickness. As noted by Govers and Wortel (2005) such oblique fault boundaries do not necessarily form proper transform plate boundaries but broad zones of distributed deformation, accommodating differential trench-parallel extension, strike-slip motion and rotation. In case the lithospheric tear propagates within the continent-ocean transition, a narrow continental margin forms highly oblique to the direction of back-arc extension. This is documented, for instance, in the Carribean, along the transcurrent Carribean-South America plate boundary (Pindell and Kennan, 2009) or on the margin of the South Orckney microcontinent, along the Scotia-Antarctic plate boundary (Dalziel et al., 2013). Despite the large-scale kinematic picture is relatively well understood, there are only few places on Earth where continental crustal deformation associated with slab-edge continental rift system can be studied both onland and offshore.

Here, we focus on the eastern Betic Cordillera, which constitutes a rifted margin defined by decreasing crustal thickness from >35 km to 20 km onshore (Diaz et al., 2016), thinning offshore to 16-6 km in the Eastern Alboran arc to back-arc region (Booth-Rea et al., 2018; Gómez de la Peña, 2020a) (**Figs 1 and 2**). This region is seen to develop above a EW-trending STEP fault at the boundary between the Alboran basin and the Iberian paleomargin (Badji et al., 2014; Gallais et al., 2013; Jolivet et al., 2021a; Mancilla et al., 2015a). The tectonic expression of the strike-slip deformation during E-W-directed crustal extension above the lithospheric tear is however controversial. On the one hand, low-angle ductile extensional detachments with a top-to-the-west sense of shear are the main features accommodating deformation in the overriding plate. Yet, a-type metamorphic domes in the lower crust, elongated parallel to the E-W direction (**Fig. 1**), formed during the early Miocene, are viewed to express the transtensional deformation at the tip of propagating tear (Le Pourhiet et al., 2012). On the other hand, E-W-directed transfer strike-slip faulting is interpreted as a late (post-middle Miocene) brittle deformation feature associated with differential E-W crustal extension between the metamorphic domes in the eastern Betics (Alpujarras fault zone ; Sanz de Galdeano and Vera, 1992; Sanz de Galdeano et al., 1985; Martínez-Martínez et al., 2006) and in the western Betics (Torcal fault zone ; Barcos et al., 2015) unrelated to ductile deformation (**Fig. 1**). In line with the latter interpretation, the dextral motion these transfer faults accommodate is assumed to be modest, reflecting a recent post-8 Ma kinematic change that accompanies the stalling of westward slab rollback, the onset of tectonic inversion in the Gibraltar Arc (Do Couto et al., 2014; d'Acremont et al., 2020; Jolivet et al., 2021a; Martínez-García et al., 2017), and progressive slab tearing and delamination of the lithospheric mantle from the eastern to the central Betics (Martínez-Martínez et al., 2006 ; Mancilla et al., 2015a ; García-Castellanos and Villaseñor, 2011; Spakman et al., 2018). Note that in a recent study the dextral displacement since 9 Ma has been estimated to more than 100 km along the Torcal fault (Crespo-Blanc et al., 2016).

The lack of structural, temporal constraints and quantification of belt-parallel motion along these faults indicates, however, that we do not yet fully understand their link with the long-term evolution of slab tearing and margin

formation. For instance, the current deformation patterns in the Central Betics, where metamorphic domes are present, brings evidence that both strike-slip faulting and extension operate synchronously (Martínez-Martínez et al., 2006). This is shown by the west-directed GPS velocities increasing westwards indicating ongoing extension, and the west-directed displacements increasing from North to South, towards the Alboran domain, revealing right-lateral shear (**Fig. 2**). This together with evidence for present-day 4.5 mm/yr westward diplacement and rotations in the Western Betics and Rif reveal that the westward slab rollback is likely to be still ongoing (Fadil et al., 2006; Gonzalez-Castillo et al., 2015). The current transtensional deformation across the Betic Cordillera is consistent with the current stress regime defined by extension direction highly oblique (max. 20°) to the Betic structural trend (or 70° spanned by the direction of extension and normal of the rift trend).
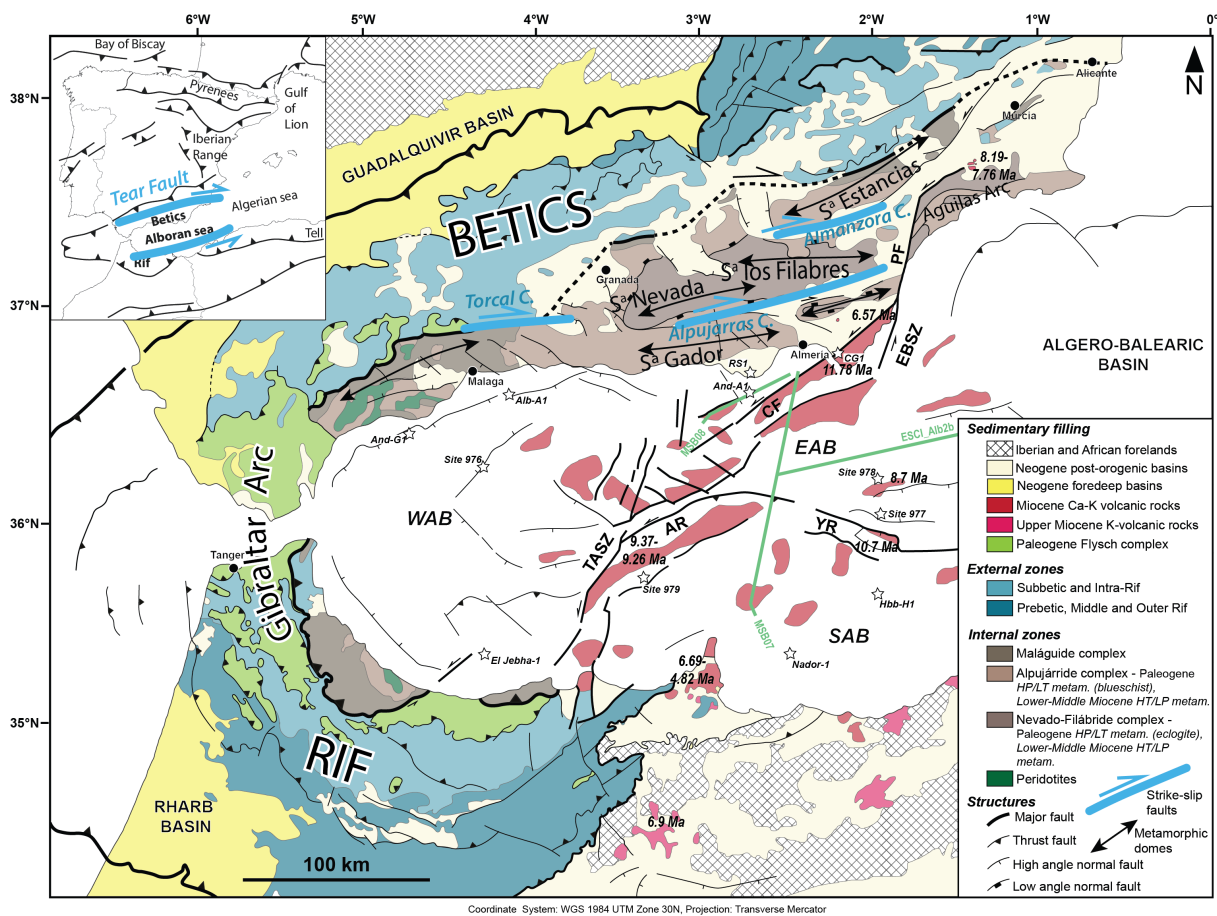
Figure 1 : Geological map of the Betic-Rif arc. Main tectonic units and age of volcanism as well as major structures and Neogene sedimentary basins are shown. The studied offshore seismic lines (red) is displayed as well as offshore wells and ODP sites (open star) for stratigraphic calibration in the East (EAB), South (SAB) and West Alboran basins (WAB). CF: Carboneras Fault; PF : Palomares Fault; AR: Alboran Ridge; YR: Yusuf Ridge; EBSZ : East Betic Shear Zone; TASZ: Trans-Alboran Shear Zone.

1.2 Highly oblique rifting triggered by slab tearing : a proof of concept in the eastern Betics

Right-lateral transtensional deformation in the Betics agrees with the extrusion model of the Alboran basin towards the Gibraltar arc to the West (Borque et al., 2019; Palano et al., 2015) caused by indentation by the east Abloran domain likely enhanced by resistance slab dragging (Spakman et al., 2018). In the East, the extrusion is accommodated by left-lateral strike-slip displacement along the Eastern Betic Shear Zone (EBSZ; Borque et al., 2019), shaped by the Carboneras Fault (CF) and Palomares Fault (PF), which separates the extrusion domain were extension and transtension is prevailing from the Águilas Arc where N-S indentation is well documented (Ercilla et al., 2022). In this region, this fault extends offshore, across the Alboran Sea, in the larger Trans-Alboran Shear Zone (De Larouzière et al., 1988; Stich et al., 2006) moving at ~4 mm/yr, equivalent to the regional 5 mm/yr NW-directed convergence between Africa (Nubia) and Europe (**Fig. 2**; Echeverria et al., 2013; Koulali et al., 2011; Nocquet, 2012; Palano et al., 2015, 2013; Vernant et al., 2010). Here, we hypothesize that the present-day oblique extension patterns is at play since the Miocene and explain the formation of the narrow Alboran rifted margin.

Only recently high-resolution 3D numerical models have been able to predict the deep structure of oblique rift domains. These models can be used as a guide to re-evaluate the evolution of the Betics. 3D models by Jourdon et al. (2021) predict that oblique extension results in narrow rifted margins, strike-slip faults and corridors coupled with subsident pull-apart basins, normal faults and block rotations (**Fig. 3**). The recognition of block rotation in the Betic arc (Crespo-Blanc et al., 2016; Platzman, 1992), strike-slip fault zones (**Fig. 1**) and NW-SE normal faulting, which defines extension direction highly oblique to the margin (Galindo-Zaldivar et al., 2003; **Figs 1 and 2**), support this view. The simulations also show that the deeper ductile crust experiences thinning (vertical flattening) and stretching perpendicular to the strike of the margin in accordance with stretching lineations parallel to the metamorphic domes and low-angle detachments (**Fig. 3**). Other types of 3D numerical experiments show that sediment loading of strike-slip faults can result in assymetric flexural basin with apparent normal fault throw (Neuharth et al., 2021) that can be mistakenly interpreted as resulting from orthogonal extension. Asymmetric basins are indeed intriguing characteristics of intramontane basins in the Betics (Rodríguez-Fernández et al., 2011; Augier et al., 2013; Do Couto et al., 2014 ; Giaconia et al., 2014). Although primarily found associated with divergent plate boundaries e.g. in the Gulf of California (Fossen et al., 2013; Fossen and Tikoff, 1998) highly oblique extension is also documented in active transform regions along the San Andreas Fault (Teyssier and Tikoff, 1998) or the North Anatolian Fault in Marmara Sea (Okay et al., 2004). A detailed analysis of highly oblique rifting deformation in the Gulf of California recognises similar tectonic elements as for the Betics, such as extensional detachment systems orthogonal to the divergence and upper crustal folds trending parallel to the divergence (Fossen et al., 2013).
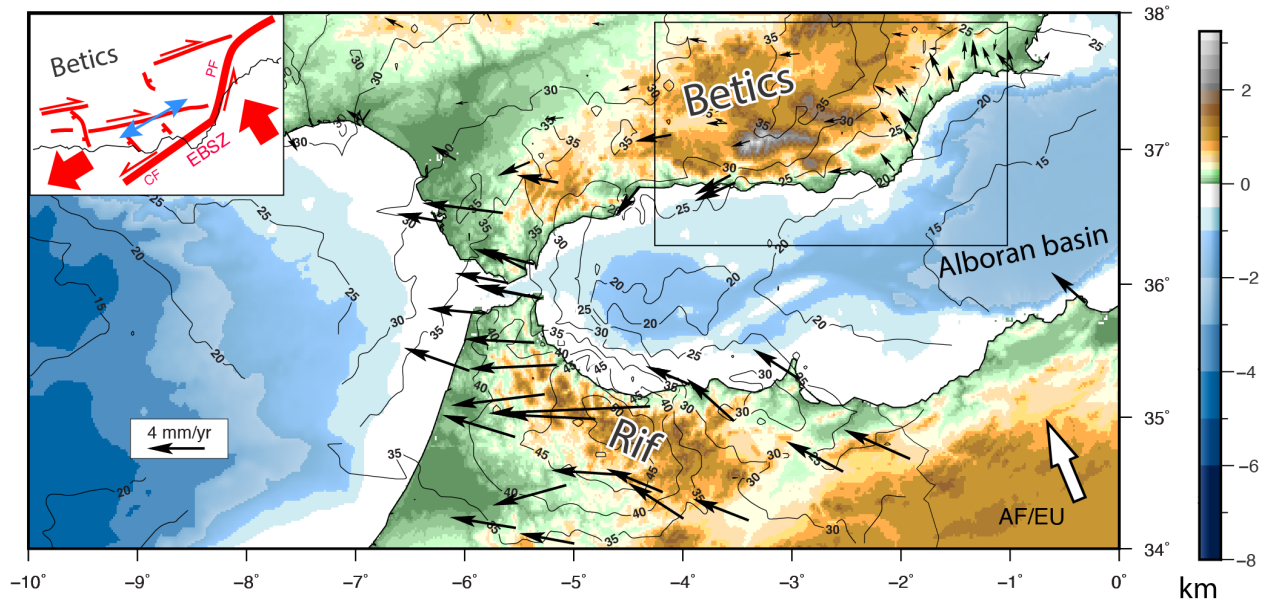
115

116 **Figure 2** : Present-day kinematics in the Betic-Rif arc and eastern Betic Cordillera (inset). GNSS-based displacements
117 in the western Alboran block and north-western Africa shown in a fixed Eurasian reference frame (black arrows after
118 Palano et al., 2015) are oblique to the AF/EU plate convergence (white arrow) inferred from plate tectonic Morvel
119 model (Argus et al., 2011). Labelled contours depict the crustal depth given in kilometers as inferred from deep seismic
120 profiles and receiver functions analysis (Diaz et al., 2016). In the eastern Betic (inset), W-directed stretching is taken
121 up by EW-directed right-lateral strike-slip fault and NW-SE normal faults. Extension direction resolved from focal
122 mechanisms (blue arrow) are after (Stich et al., 2006). CF: Carboneras Fault; PF : Palomares Fault; AR: Alboran
123 Ridge; YR: Yusuf Ridge; EBSZ : East Betic Shear Zone; TASZ: Trans-Alboran Shear Zone.

124

125 Several tectonic features need further discussion however. First, the relevance of strike-slip faulting in the past is

126 debatable as only a few occurrence of crustal-scale strike-slip faults are mapped (**Fig. 1**). Second, the detail of the

127 temporal and spatial relationships between the formation of the oblique/transform margin and STEP faulting remain

128 elusive. We here review the temporal and spatial evolution of Neogene intramontane sedimentary basins and related

129 brittle deformation in the eastern Betics. In addition, we exploit offshore seismic reflection lines to propose a new

130 crustal-scale section across the oblique margin. Based on these constraints we present a tectonic scenario for the

131 formation of the high-obliquity rifted margin controlled by STEP faulting.

132
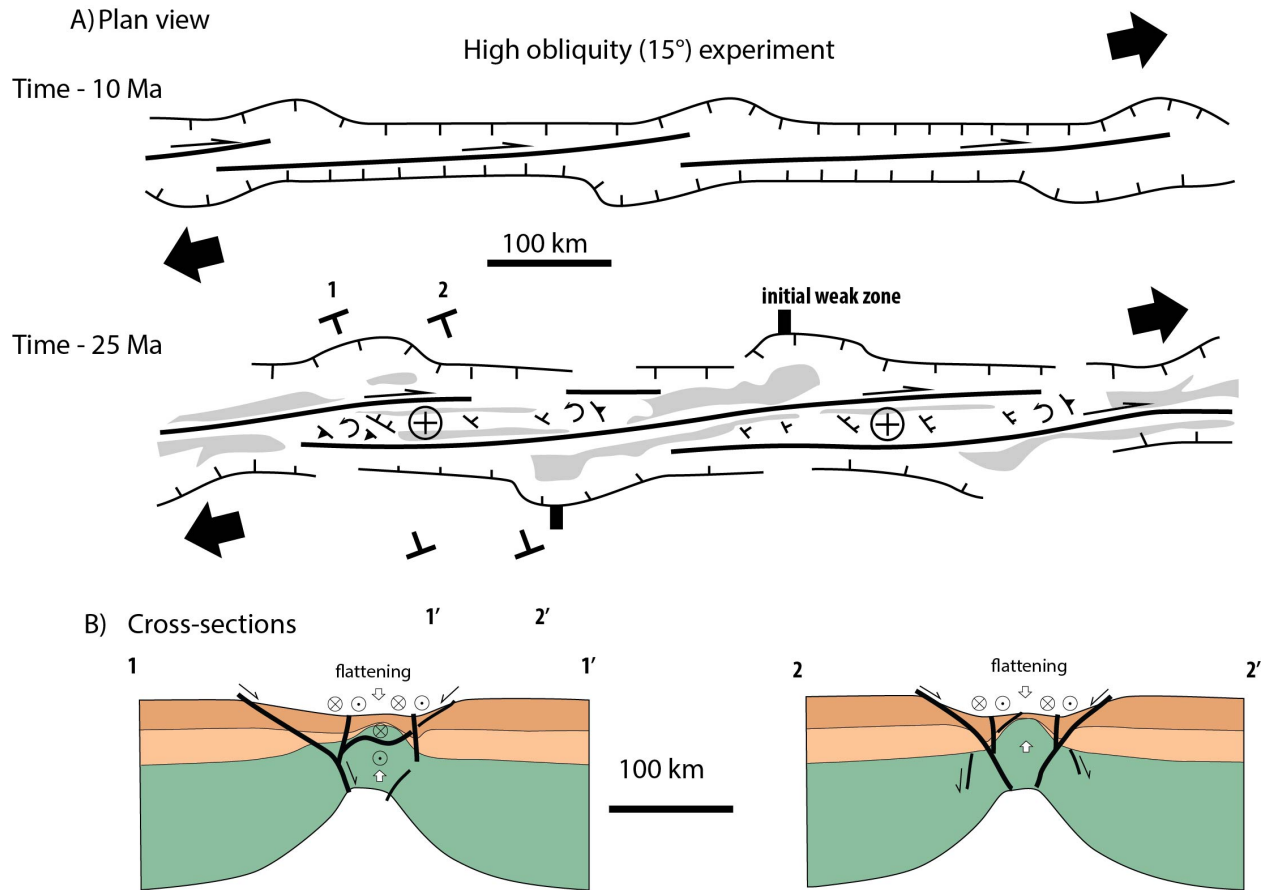
Figure 3 : Sketch of highly oblique rift experiments based on the results of a 3D thermo-mechanical model (Jourdon et al., 2021). Results are depicted in plan view (A) and cross-sections (B) for two steps (after 10 Myrs and 24 Myrs) for the case where extension is set with an angle of 15° with respect to the rift axis. Grey regions in (A) are basins adjacent to uplifted domains (cross-circle symbol) associated with right-lateral strike-slip faults. Cross-sections (B) depict the abrupt crustal thinning that occur perpendicular. Crustal thining is most visible for the lower crust and produces the formation of an abrupt necking domain controlled by rift-parallel normal faults dipping towards the center of the rift and right-lateral strike-slip faults.

2. Geodynamics and STEP faulting in the Betics

The onset of N-directed movement of Africa, by the Late Cretaceous-Paleogene, led to far-field, Laramide-like contraction from Morocco throughout Western Europe (Mouthereau et al., 2021). South of Iberia, in the Betic-Rif domain, the closure of hyper-extended rift systems and oceanic basins of the Atlantic-Alpine Tethys resulted in the development of a proto-Betic accretionary prism, likely largely submerged (Angrand and Mouthereau, 2021; Daudet et al., 2020; Vergés and Fernàndez, 2012). By about 50 Ma, the acceleration of plate convergence led to the shortening of continental rift and oceanic basins and topographic uplift all over Iberia (Daudet et al., 2020; Mouthereau et al., 2021, 2014; Rat et al., 2019; Vacherat et al., 2016; Waldner et al., 2021) associated with the onset of continental rifting along the Western European Rift (e.g. Mouthereau et al., 2021). 35 Ma ago, as Africa convergence slowed down, the western Mediterranean sea opened accompanied by retreating slabs (Dewey, 1988; Dewey et al., 1989; Faccenna et al., 2014; Jolivet and Faccenna, 2000; Rosenbaum et al., 2002). Subduction occurred mainly before 30 Ma as argued by age constraints on high-pressure mineral assemblages (Augier et al., 2005a; Bessière et al., 2021; Booth-Rea et al.,

154   2015; Gomez-Pugnaire and Fernandez-Soler, 1987; Platt and Vissers, 1989; Platt and Whitehouse, 1999) and has been

155   suggested to last until the mid-Miocene in the eastern Betics e.g. (Platt et al., 2013). The timing of formation of the

156   Alboran basin is constrained to 23 to 16 Ma by the oldest deposits found on Alboran basement and by the timing of

157   high-temperature metamorphic overprint and rapid cooling to shallow crustal temperature (Bessière et al., 2021;

158   Daudet et al., 2020; Janowski et al., 2017; Johnson et al., 1997; Platt et al., 2005; Sosson et al., 1998; Vázquez et al.,

159   2011; Zeck et al., 1992). The eastern Alboran basin formed later, mostly by late Miocene arc magmatism (Booth-Rea

160   et al., 2007; 2018; Gómez de la Peña et al., 2020a).

161   All kinematic reconstructions agree that extension results from the westward migration of the arc front and retreat of

162   the Alboran slab, well imaged below the Gibraltar arc as a steeply-dipping high-velocity anomaly (Bezada et al., 2013;

163   Heit et al., 2017; Mancilla et al., 2018, 2015a, 2015b; Palomeras et al., 2014; Spakman and Wortel, 2004; Villaseñor

164   et al., 2015). These reconstructions, however, differ according to the paleo-position of Alboran terrane, and hence to

165   the amount and vergence of subduction (Angrand and Mouthereau, 2021; van Hinsbergen et al., 2014; Lonergan and

166   White, 1997; Romagny et al., 2020; Rosenbaum et al., 2002; Vergés and Fernàndez, 2012). Seismic tomography

167   reveals that slab detachment and tearing occur along the conjugate Alboran margins of the southern Betics and

168   northern Africa (Govers and Wortel, 2005; Heit et al., 2017; Mancilla et al., 2015a; Meighan et al., 2013; Spakman

169   and Wortel, 2004).

170   In **Fig. 4** we refer to the reconstruction of Angrand and Mouthereau (2021) that has the advantage of reconciling

171   previous western Mediterranean models (Romagny et al., 2020; Vergés & Fernàndez, 2012) with recent

172   thermochronological analyses in western Betics (Daudet et al., 2020) and other geological data (see compilation in

173   Mouthereau et al., 2021). This model considers that the Alboran domain has been rifted from Iberia during the Jurassic.

174   It is in agreement with detrital and igneous zircon U-Pb ages that suggest Alboran was attached to Iberia in the late

175   Paleozoic (Jabaloy-Sánchez et al, 2021). It also accounts for the existence of an upper Cretaceous-Paleogene foreland

176   basin that formed adjacent to a proto-Betic orogen and in continuity eastwards with the Balearic Promontory. In that

177   respect, it contrasts with other models placing the Alboran domain to the south of the Balearic Promontory (Moragues

178   et al., 2021; van Hinsbergen et al., 2014).

179   In this reconstruction about 400 km of slab retreat is estimated since about 35 Ma (gray path, blue arrows in **Fig. 4**).

180   It is worth noting that for Romagny et al. (2020) a similar amount (i.e. 400 km) is accommodated by back-arc extension

181   of the Alboran crust, implying the same magnitude of displacement along the STEP fault in the Betics. In the

182   reconstruction of Angrand and Mouthereau (2021), however, crustal thinning in Alboran basin is linked to

183   delamination retreat of the Alboran lithospheric mantle towards the west. Because of the decoupling between crust

184   and mantle, the length of the delaminated slab resolved at depth in seismic tomography, should not be simply translated

185   into the amount of E-W crustal extension in the Alboran domain. This further implies that the displacement across the

186   STEP fault must be also less than 400 km. Daudet et al. (2020) suggested that an extension of 110 km estimated from

187   the restoration of low-angle detachment systems in the central and eastern Betics (Martínez-Martínez et al., 2002) is

188   likely to be a more accurate crustal estimate of the movement Alboran domain rather than the total slab length.

189
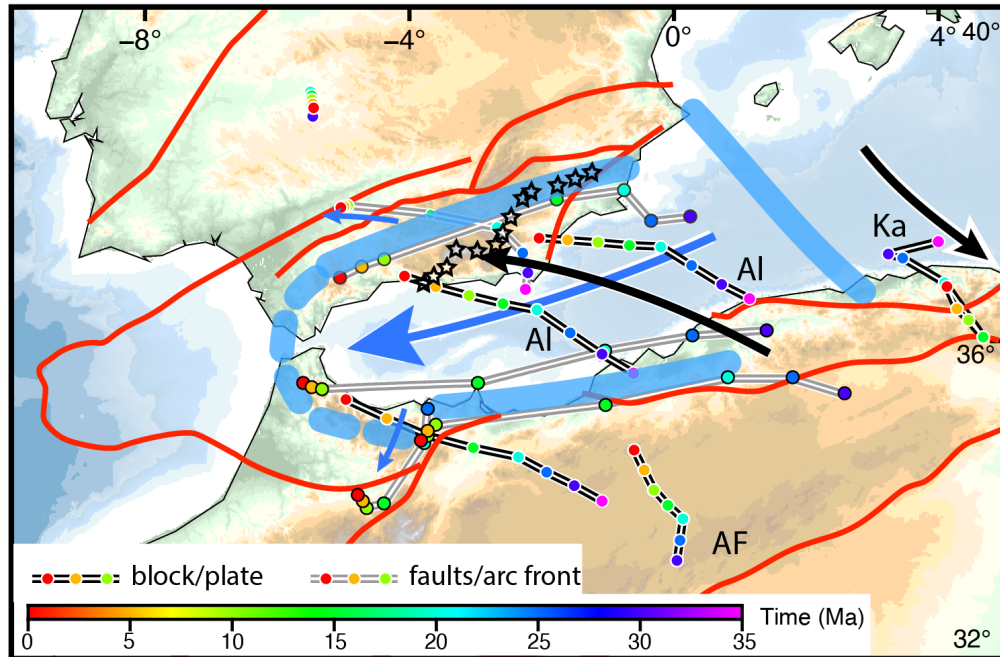
Figure 4: Kinematics of African plate (AF), Alboran (Al) and Kabylides (Ka) blocks with respect to fixed European plate since 35 Ma reconstructed after Angrand and Mouthereau (2021). Thick blue lines depicts the approximate position of lithospheric tear faults (between Al and Europe and Africa) and transfer faults (between Al and Ka). Tear faults located in Betics and Rif are after Jolivet et al. (2021b). Black stars depicts the positioned of tear fault in the Betics as defined by Mancilla et al. (2015a). Black arrows indicate the movement of Al and Ka with respect to Europe along black motion paths presented from 35 Ma to present. Grey motion paths refer to the motion of specific structures relative to Europe, including the motion of the arc front (thick blue dashed line) and faults in red. Dark blue arrow depicts the movement of the arc front due to retreating delamination towards the west.

3. Miocene extension in the eastern Betics

3.1 Relationships between domes and basins : from transtension and pure extension to late tectonic inversion

The most prominent extensional features in the eastern Betics are : 1) E-W elongated ranges that formed metamorphic domes with foliations bearing prominent E-W stretching lineations, for instance, in the Nevado-Filabrides Complex (**Fig. 5**; e.g. Sierra de los Filabres, Sierra Nevada, and the Sierra de las Estancias) and Serravallian-Tortonian sedimentary basins (Tabernas-Sorbas, Alpujarras, Almanzora and Huércal-Overa basins); 2) NNW-SSE/NW-SE normal fault systems and basins oblique to the domes such as the NW-SE trending Guadix-Baza and Alhabia basins (Galindo-Zaldivar et al., 2003; Martínez-Martínez and Azañón, 1997) (**Fig. 5**). They are described as asymmetric half grabens (Do Couto et al., 2014; Martínez-Martos et al., 2017; Pedrera et al., 2010, 2009) formed during the Upper Serravallian-Early Tortonian (Augier et al., 2005b; Augier et al., 2013; Meijninger and Vissers, 2006). Several of these NW-SE faults are active and cut across the metamorphic domes and the sedimentary basins (Augier et al., 2005a; Booth-Rea et al., 2004a; Giaconia et al., 2012; Montenat and Ott d'Estevou, 1999).

In addition to these structures, there are E-W right-lateral strike-slip fault zones and parallel depressions, like the Alpujarras fault zone between the Sierra de Gádor and the Sierra Nevada, and the Almanzora fault zone between the Sierra de los Filabres and Sierra de las Estancias (**Fig. 5**). The left-lateral Carboneras and Palomares fault system

215 (Reicherter and Hübscher, 2006; Scotney et al., 2000) marks the tectonic limit with the Cabo de Gata volcanic province

216 (**Fig. 5**).

217 The domes are extension-related features interpreted either as 1) EW-metamorphic domes resulting from the

218 exhumation in the footwall of a regional W-directed extensional low-angle detachments, later folded during post-

219 Tortonian N-S contraction (Martínez-Martínez and Azañón, 1997; Martínez-Martínez et al., 2002, 2004) or 2)

220 Miocene metamorphic domes formed by constrictional ductile strain regime accompaniying W-directed stretching of

221 the Alboran domain and trench retreat, with limited overprint by the Tortonian contraction ca. 8 Ma (Augier et al.,

222 2013; Augier et al., 2005; Augier et al., 2005b; Galindo-Zaldivar et al., 2015; Jolivet et al., 2021b; Martínez-Martínez

223 et al., 2002). Low-temperature constraints from the Nevado-Filabride and Alpujarride complexes confirm the west-

224 directed exhumation of the basement that occurred progressively from the Sierra de los Filabres at ~13-11 Ma

225 (Serravallian) in the East to the Sierra Nevada at 8-6 Ma (Late Tortonian-Messinian) in the West (Clark and Dempster,

226 2009; Janowski et al., 2017; Johnson et al., 1997; Platt et al., 2005; Reinhardt et al., 2007; Vázquez et al., 2011).

227
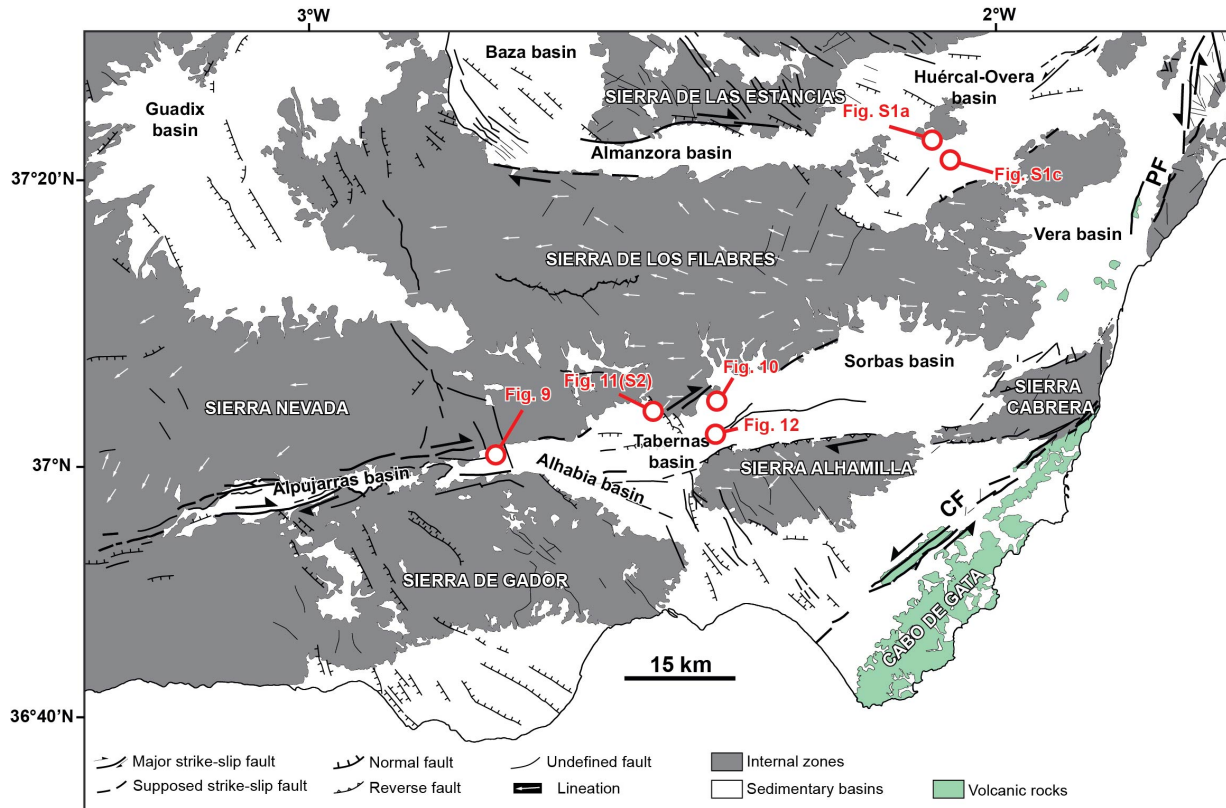
229 **Figure 5** : Tectonic map of the eastern Betics showing the main structural elements in black after Augier et al. (2005)
230 and Do Couto (2014). CF: Carboneras Fault; PF : Palomares Fault.

231

232 Tectonic models for the formation of Neogene intramontane sedimentary basins vary depending on the prevailing

233 tectonic regime. EW-directed basins have been early described as pull-apart basins (e.g Alpujarran fault zone; Sanz

234 de Galdeano et al., 1985). Structural analyses then led to re-interpret these structures as transfer zones resulting from

235 differential extension between exhuming core-complexes (and detachment systems) since the Serravallian (13-11 Ma)

236   later refolded during Tortonian (9-8 Ma) compression in the Eastern Betics while extension is still active in the Central

237   Betics (Martínez-Martínez et al., 2006). Other authors proposed that NE-SW extension lasted until 7.5-7 Ma in the

238   Eastern Betics (Booth-Rea et al., 2004b; Giaconia et al., 2014).

239   In support to the compressional stress regime in the Eastern Betics, Martínez-Martos et al. (2017) interpreted the E-

240   W depressions are related to the tectonic reactivation of crustal weakness zone as dextral strike-slip faults in a

241   counterclockwise rotation, accommodating part of the the N-S shortening. There are evidence that at the end of the

242   Tortonian a regional uplift occurred, rising the remnants of late Tortonian marine platform, 7.2 Ma in age, to 1600 m

243   above sea level in the Sierra de Gádor (Braga et al., 2003; Janowski et al., 2017), coincidently with the onset of

244   contraction in the Sierra Alhamilla and Sierra de los Filabres (e.g. Do Couto et al., 2014), in the Alboran domain (e.g.

245   Martínez-García et al., 2017) and on the margins of the eastern Betic (Giaconia et al., 2013 ; 2015). In addition to

246   shortening, this recent uplift may reflect deep mantle mechanisms like slab tearing or delamination (e.g. Duggen et

247   al., 2003; García-Castellanos and Villaseñor, 2011; Mancilla et al., 2015a).

248   Based on the prevalence in some EW-trending basins, like the Huércal-Overa basin, of EW-trending normal faults,

249   these basins have alternatively been interpreted as resulting from late exhumation stage of the domes, possibly as soon

250   as the Serravallian, but mostly after the early Tortonian (syn-sedimentary faulting) (Augier et al., 2013; Augier et al.,

251   2005b; Meijninger and Vissers, 2006). The NW-SE/NNW-SSE sedimentary basins (Guadix, Baza, Alhabia; **Fig. 5**),

252   in contrast, are extensional basins formed parallel to the direction of the regional compression (Sanz de Galdeano and

253   Vera, 1992; Larouzière et al., 1988). E-W strike-slip fault zones, aligned in the direction of the domes, and NW-SE

254   normal faulting patterns are both key features consistent with predictions from models of oblique extension at

255   transform margin (**Fig. 3**). Yet, based on existing structural and tectonic syntheses a clear temporal relationships

256   between E-W ductile stretching in the domes and transcurrent deformation is not established (**Fig. 5**).

257

258   **3.2 Is the Tortonian rift-related subsidence consistent with oblique extension ?**

259   The stratigraphic architecture and depositional evolution of Tortonian intramontane basins provides first-order

260   informations on the distribution of crustal thinning. Among the oldest sediments deposited unconformably on the

261   Paleozoic-Triassic basement are the red alluvial conglomerates and deltaic series dated from the Serravallian to the

262   Lower Tortonian (**Fig. 6a**). They are thicker and well exposed on the flanks of the Almanzora basin and on the northern

263   Huércal-Overa basin (HOB), compared to the Alpujarras Corridor (AC) and Tabernas basin (TB) (**Figs. 6 and 7a**;

264   Augier et al., 2013; Pedrera et al., 2010, 2007; Poisson et al., 1996). In the east of the Sorbas basin, it should be noted

265   that Langhian-Serravalian deposits and perhaps sediments as old as Burdigalian have been locally reported (Giaconia

266   et al., 2014).

267   Paleogeographic reconstructions indicate that these Serravallian to Lower Tortonian sediments were deposited on a

268   large emerged domain, stretching from Huercal-Overa to Granada, in the West and in Tabernas, to the South (Braga

269   et al., 2003). Sourced from the Nevado-Filabride metamorphic complex (Hodgson and Haughton, 2004; Kleverlaan,

270   1989; Meijninger and Vissers, 2006; Pedrera et al., 2010, 2007; Pickering et al., 2001; Weijermars et al., 1985) these

271   deposits mark the onset of surface exhumation of the Sierra de Las Estancias and Sierra de Los Filabres.

272   During this intial stage, HOB is the most subsident basin (**Figs. 6b, 7a and 7b**), accumulating sediments at rates of
273   400 m/Ma while rates are 140-180 m/Ma in the Tabernas basin (**Fig. 6b**) (Augier, 2005). Higher subsidence in the
274   HOB, which also started earlier than in other basins, suggests extension occurred originally to the North associated
275   with the exhumation of the Sierra de Las Estancias. Basal continental conglomerates are overlain by grey coarse-
276   grained Tortonian sandstones found occasionally, e.g. in the Almanzora basin, intercalated with marine marls (**Figure
277   6a**). They are topped by mid-Tortonian bioclastic calcarenite and coral reefs (Braga et al., 2003; Martin et al., 1989;
278   Pedrera et al., 2007).

279   During the same interval, TB recorded the deposition of 300 to 400 m of coarse to medium-grained deltaic marine
280   clastics overlying unconformably the lowermost red series (**Fig. 6a**). These sediments pass upwards, e.g. in TB, to
281   deeper marine 1200 m-thick turbiditic and marls series intercalated with regional-scale megabeds, revealing the onset
282   of rapid tectonic subsidence (Haughton, 1994; Kleverlaan, 1989, 1987; Pickering et al., 2001; Weijermars et al., 1985).
283   Details of depositional architecture of the Tortonian suggest that part of this subsidence evolution was controlled by
284   E-W dextral strike-slip faults (Haughton, 2000 ; Baudouy et al., 2021) under transtensional strain.

285   The transition from continental to deep marine sedimentary environments (water depth of 400-600 m according to
286   Poisson et al., 1999) witnesses the rapid rift-related tectonic subsidence achieved during the upper Tortonian times
287   (~9 Ma; **Figs. 6** and **7c**) (Augier et al., 2005b; Montenat and Ott d'Estevou, 1992; Weijermars et al., 1985). At around
288   8 Ma, accumulation rates drop by a factor of two to 200 m/Ma in HOB and 70 m/Ma in TB, revealing a marked
289   reduction in subsidence. Subsidence then became negative as basement uplifted from around 7 Ma (**Figs. 6b** and **7d)**
290   in both TB and HOB.

291

292

293
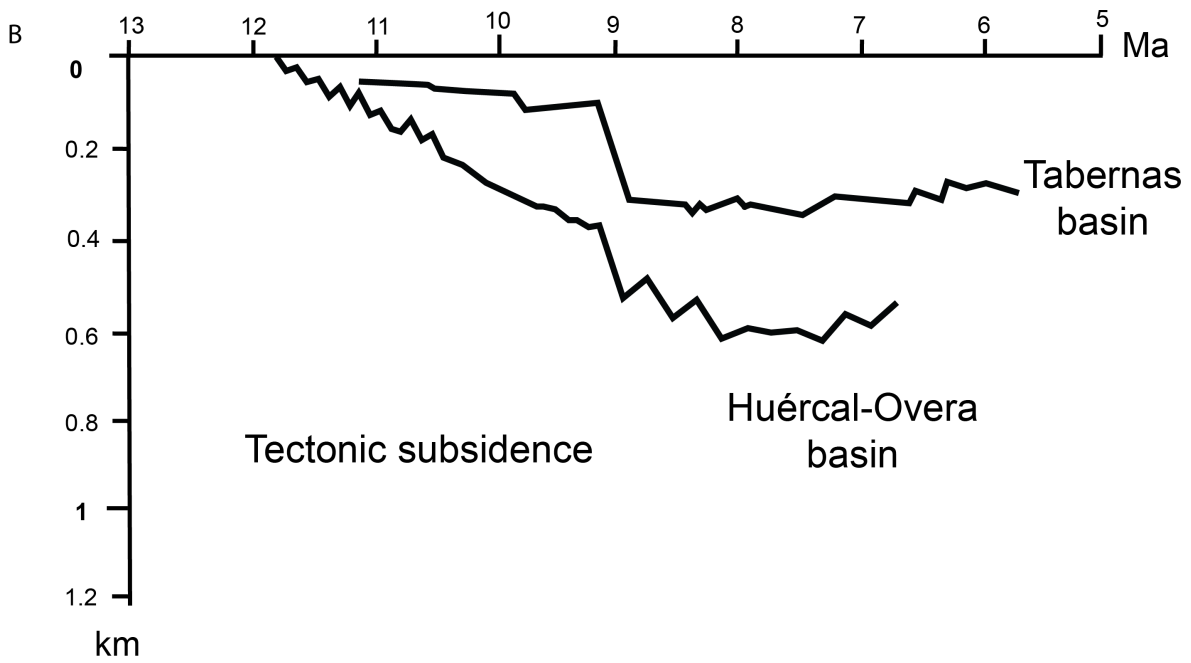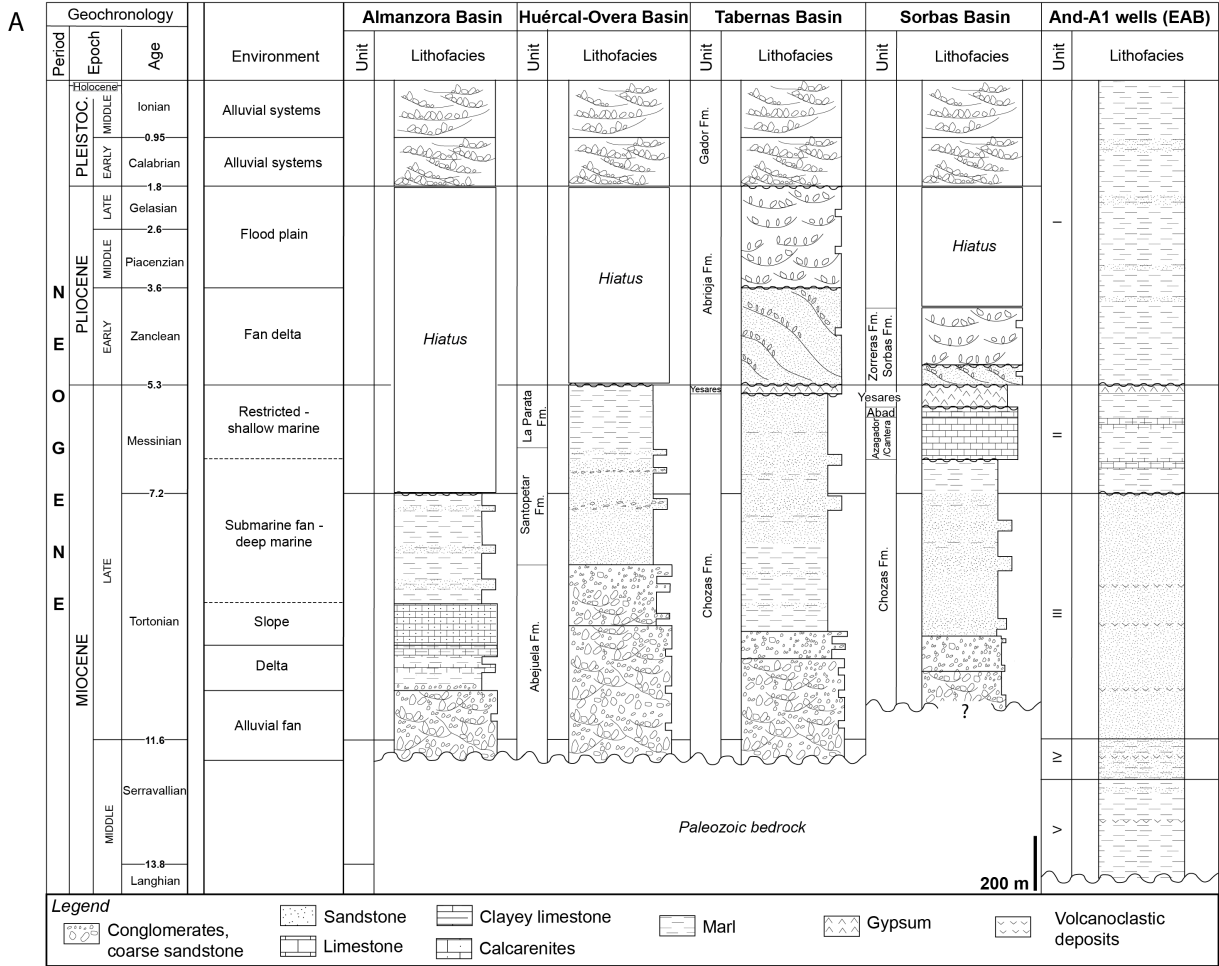
294   **Figure 6** : Stratigraphic evolution and lithologies of intramontane basins in the eastern Betics and offshore A1 well.
295   (a) Neogene stratigraphy and basin-fill correlation in the Almanzora and Huercal-Overa basins (Mora, 1993), Tabernas
296   basin (Hodgson and Haughton, 2004; Kleverlaan, 1989; Pickering et al., 2001) and Sorbas basin (Fortuin and
297   Krijgsman, 2003; Martín and Braga, 1994; Riding et al., 1998). Middle Miocene sedimentary environments in the
298   Alboran Sea are after (Comas et al., 1992). (b) Neogene tectonic subsidence evolution for Tabernas basin and Huércal-
299   Overa basin are from Augier (2004). The curves are obtained from backstripping techniques incorporating eustatic
300   and paleobathymetric corrections. Question mark beneath the Sorbas basin lithofacies column indicates the potential
301   for uncertainty/variability across the basin (see text).
302

303   The geometry of the Almanzora (Pedrera et al., 2009), Sorbas (e.g. Do Couto et al., 2014) and Huércal-Overa basin

304   basins (Pedrera et al., 2010) inferred from gravity measurements indicate that these basins are asymmetrical and

305   deepening southwards. This sediment infill pattern recalls the formation of asymmetrical basins predicted by

306   numerical models of flexural strike-slip basins (Neuharth et al., 2021). According to this model, the asymmetry

307   observed should reflect the developement of strike-slip basins loaded by sediments originated from the North. In

308   addition, a larger subsidence in HOB is an indication of abrupt crustal thinning to the south of Sierra de las Estancias

309   where the crustal thickness is the largest (**Fig. 2**). Therefore, at least the Serravallian-Tortonian infill patterns agree

310   with oblique extension.

311
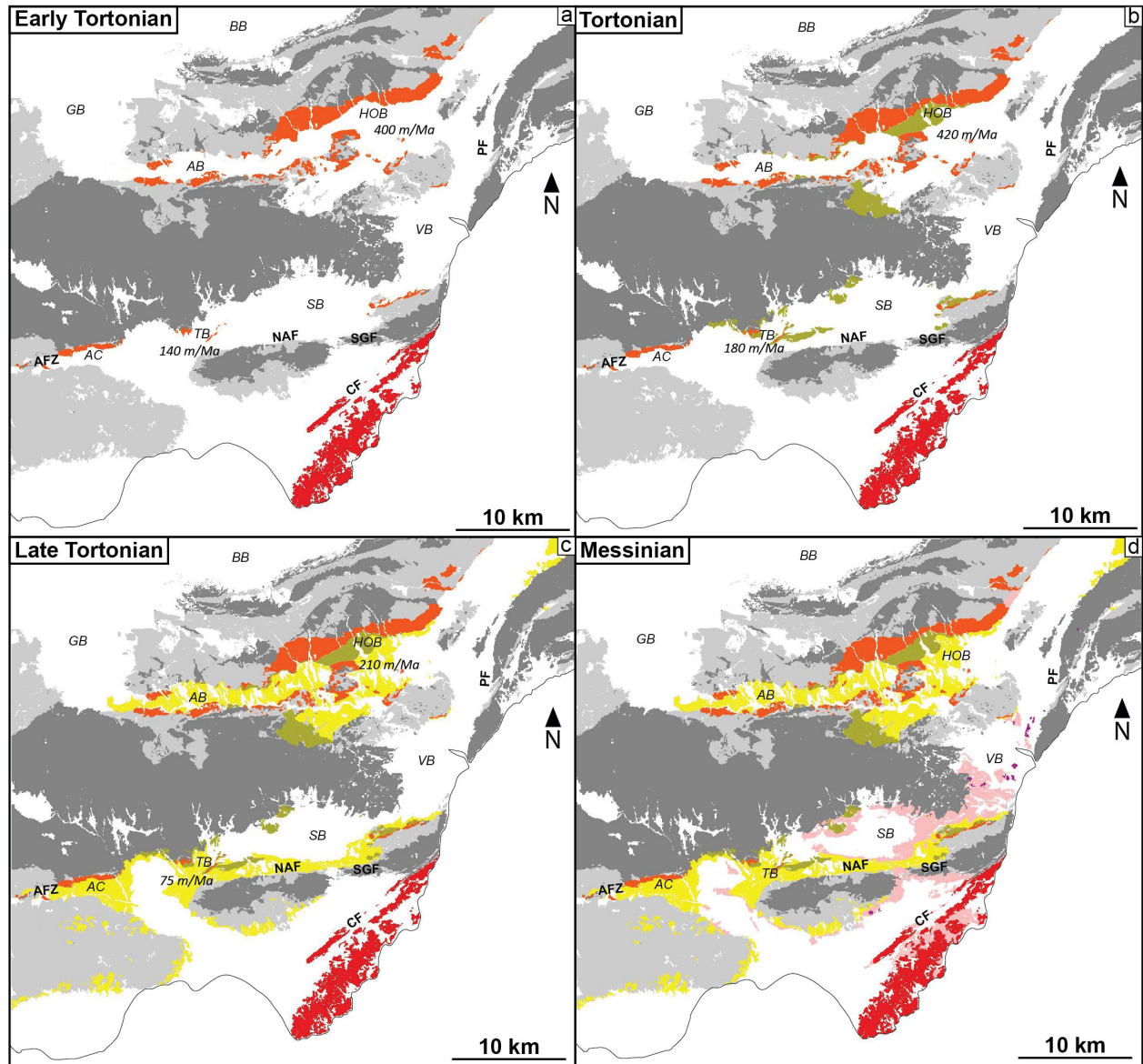
Figure 7: Distribution of (a) lower Tortonian, (b) Tortonian, (c) upper Tortonian and (d) Messinian deposits based on geological mapping of the different basins. CF: Carboneras Fault; PF : Palomares Fault; SGF: South Gafarillo fault; NAF: North Alhamilla fault; AFZ: Alpujarras fault zone; BB: Baza basin; GB: Guadix basin; AB: Almanzora basin; HOB: Huercal-Overa basin; VB: Vera basin; SB: Sorbas basin; TB: Tabernas basin; AC: Alpujarras Corridor.

4. Brittle faulting : pure extension versus transtensional deformation in Neogene basins

4.1. Tectonic regime in the eastern Betics

Figure 8 presents a compilation of 112 fault slip data inversion previously analysed in the eastern Betics combined with new measurements conducted in the Alpujarras Corridor and in the Tabernas basin (**Table S1**). Most faults are syn-Tortonian or cut through the Tortonian. This compilation emphasizes a regional trend of σ3 stress axes oriented

323 NNE-SSW (N20°E) with subbordinate σ3 oriented E-W. In details, this well-defined regional horizontal extension

324 reflects a combination of pure normal faulting regime (σ2 horizontal and oriented NW-SE/WNW-ESE, 73% of stress

325 tensors) and strike-slip faulting regime (σ2 vertical to steeply-dipping and σ1 horizontal an striking NNW-SSE, 27%

326 of stress tensors). N-S to NW-SE compression is also reported in the HOB associated with incipient synform and

327 depocenter which is dated to the lower Tortonian coeval with the prominent EW/WSW-ENE extension (e.g. Pedrera

328 et al., 2010).

329 We describe below, based on a selection of oucrops in the vicinity of the contact between Tortonian basins and major

330 metamorphic domes, the expression of EW and NW-SE extensional faulting in the field. We then discuss how they

331 are linked to the regional stress regimes.

332

333
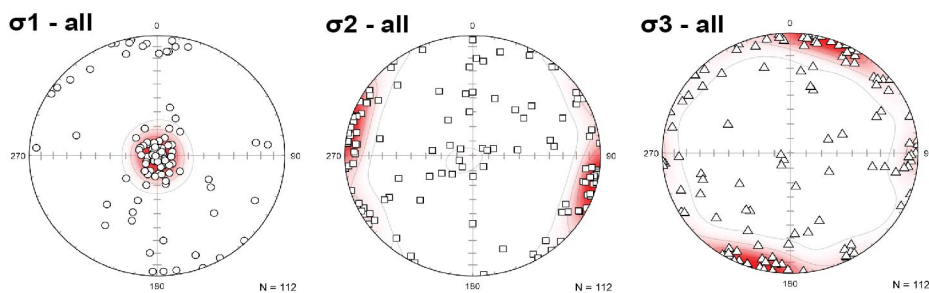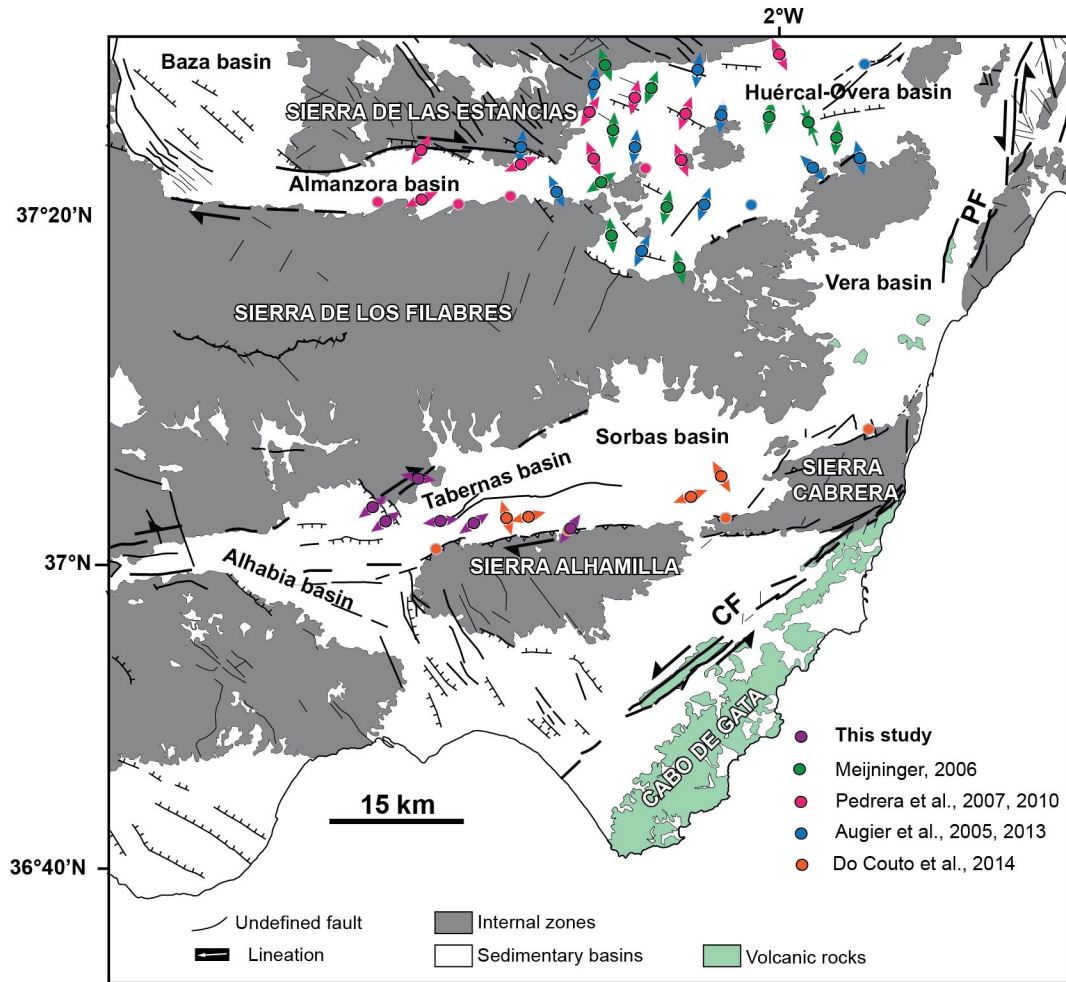
Figure 8: Synthesis of stress regimes resolved from fault slip data inversion in Tortonian basins. Color-coded circles with arrows depict tectonic sites where extension (given as arrows) is horizontal (pure extensional or strike-slip stress regimes). Sites where reverse tectonic regimes prevail are shown as circles highlighted in grey. Below, stereoplots of paleostresses σ1, σ2 and σ3 show a compilation of all brittle tectonic regimes extracted from Table S1. Collectively they define a prominent extension oriented NNE-SSW with a subordinate E-W-striking extension. CF: Carboneras Fault; PF : Palomares Fault.

340

4.2 EW-trending faults: evidence for pre-Tortonian oblique extension ?

In Tortonian intramontane basins, one of the main set of faults is represented by E-W-directed faults, including ENE-WSW to ESE-WNW sets. North of the Alpujarras Corridor (AC), 3 km to the NE of Canjáyar, the contact between the basal Tortonian conglomerates and the series of Alpujarride complex is exposed in the Rambla de Tices. It is

345   shaped by a 2-meter thick fault zone (**Figs. 9a,b**) striking N100°E, which has a normal sense of slip with a right-lateral

346   strike-slip component (**Fig. 9c**). It consists of cataclastic breccias and sheared blocks (boudins) of the host rocks (**Fig.**

347   **9d**). This major fault is found along the 65 km-long Alpujarras fault zone described by Martínez-Martínez (2006) as

348   a major strike-slip dextral transfer zone south of the Sierra Nevada that acommodates both WSW-extension and dextral

349   movement. It is mechanically consistent with NE-SW/ENE-WSW extension under a strike-slip regime as resolved

350   nearby along the same faults system (Martínez-Martínez, 2006). **Fig. 9** indicates the fault is parallel to the basal

351   Tortonian series but cuts across the Alpujarride complex. In the HOB, on the southern flank of the Sierra Limaria

352   (**Fig. 8**), the unconformity between the lower Tortonian red conglomerates and the Alpujarride units (Rambla de

353   Cordoba, 2km NW Arboleas, **Figs. S1a, b**) is found reactivated as a normal fault with a dextral shear component.

354   To the North of TB, a large morphological surface presents a rare exposure of the micaschist basement of the Nevado-

355   Filabrides complex allowing the study of deformation on the southern flank of the Sierra de los Filabres (**Fig. 10**). The

356   deformed NF series shapes a kilometric-size antiform with axial planar surface dipping towards the North. The steeply-

357   dipping cleavages directed NE-SW on its southern flank are deformed by numerous dextral shear zones with lengths

358   ranging from 100 m to less than 5 m (**Fig. 10b, c**). In addition to isoclinal folds parallel to the main foliation that are

359   clearly associated to an early stage of ductile EW-stretching, we recognize close to the strike-slip shear zones, steeply-

360   dipping metric-size open to tight folds inclined to the NE (**Fig. 10d**). To the south, Tortonian conglomerates are

361   overlying unconformably the folded NF foliation. This stratigraphic relationships and the average low dip of Tortonian

362   strata (20°SE) indicate that strike-slip deformation occurred before the deposition of Tortonian conglomerates and

363   after the tilting of the NF foliation (see cross section in **Fig. 10a**). This argues that the transition from HP

364   metamorphism (Burdigalian-Langhian) in the NF (Platt et al., 2006) to W-directed ductile crustal thinning and right-

365   lateral strike-slip faulting occurred before the Tortonian, most likley around the Serravallian at 12-13 Ma. This interval

366   is considered to mark the transition from ductile to brittle extension in the region (e.g. Augier et al., 2013). Because

367   strike-slip faulting postdates folding of the NF foliation, and are consistent with WSW-ENE oblique extension, we

368   suggest that the Sierra de los Filabres metamorphic dome formed in a transtensional strain regime. This hypothesis

369   conforms with prediction of transtension at the tip of the STEP fault (Le Pourhiet et al., 2012) and with model of

370   oblique extension (see **Fig. 3**).

371
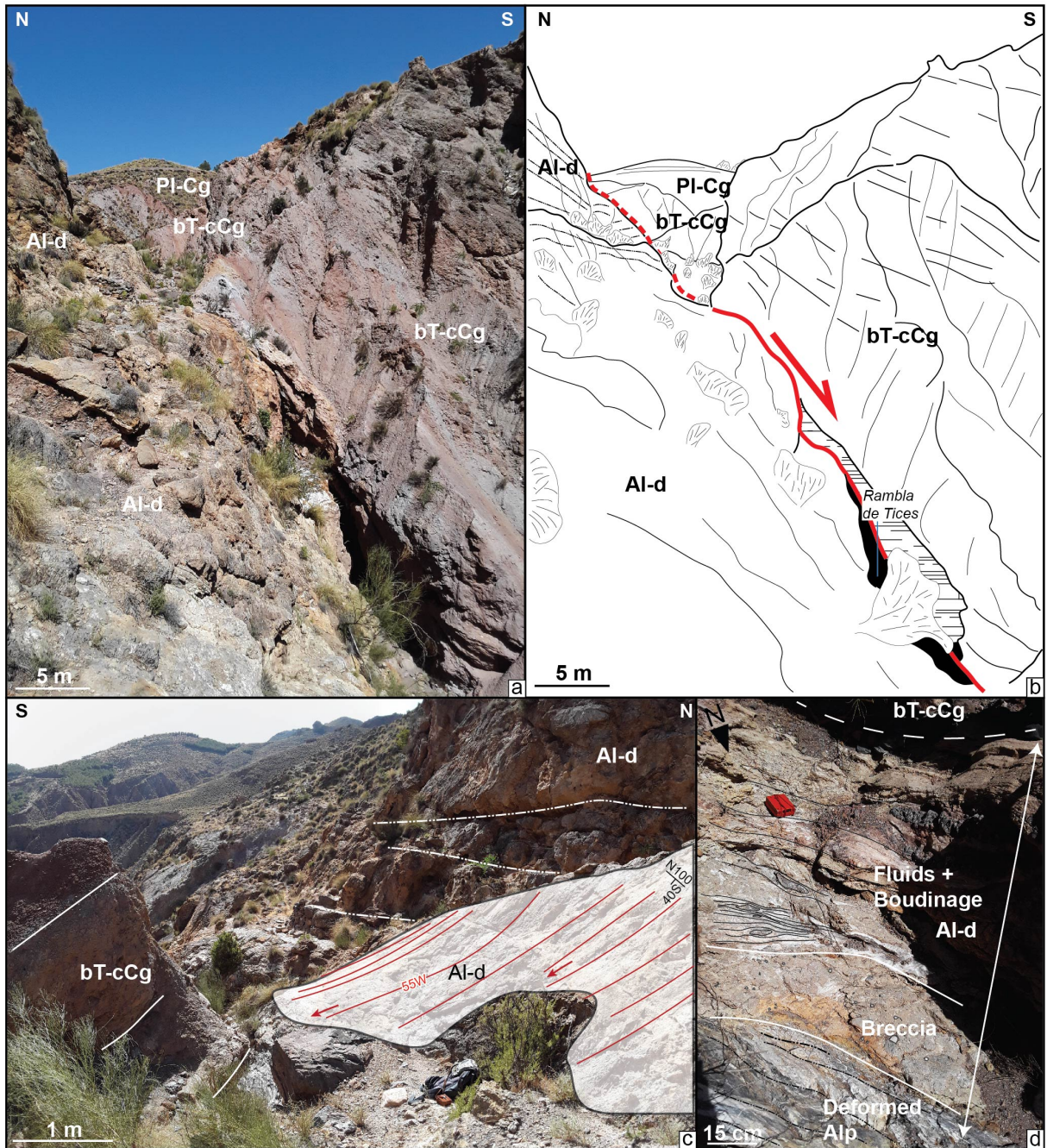
372

373 **Figure 9**. (a) and (b) Fault zone at the contact between the Tortonian basal conglomerates and the series of the
374 Alpujarride complex south of AC (Rambla de Tices, see **Fig. 5** for location). (c) slikenslides on the fault zone reveasl
375 a normal sense of slip with right-lateral strike-slip component found in association with (d) cataclastic breccias,
376 sheared boudins of metamorphic and sedimentary rocks. Al-d: Alpujarride dolomites; bT-cCg: basal Tortonian
377 continental Conglomerates; Pl-Cg: Pliocene Conglomerates. Coordinates 37.031944°N/-2.716274°E.

378

379 **4.3. NW-SE-trending normal faults**

380 A second set is represented by NW-SE directed normal faults (**Fig. 8**). They are found, for instance, bordering the the

381 NE part of Alhabia basin, where they cut across the basement and interrupt the westward continuity of the southern

382   flank of the Sierra de los Filabres. One major fault zone of this system is well exposed in the Arroyo del Verdelecho,

383   7 km to the west of Tabernas, on the eastern border of the Alhabia basin (**Figs. 11 and S2**). From a regional point of

384   view this large NW-SE fault zone controls the deepening of the Tortonian basin and the position of Pliocene

385   depocenter in its hangingwall, towards the West. NW-SE normal faults also cut across the lower Tortonian

386   conglomerates in the hanginwall but their throw diminishes upward in the upper Tortonian margin sediments,

387   suggesting fault activity during the late Tortonian (**Fig. 11**). One major fault zone is outlined by cataclastic breccias

388   made of marbles originated from the exhumed Alpujarride complex in the Sierra de los Filabres (**Fig. S2**).

389   South of HOB (south of Arboleas), NW-SE faults are seen cutting through the late Tortonian sands and marls series,

390   indicating that NE-SW extension is at least Tortonian (**Figs. S1c, d**).

391
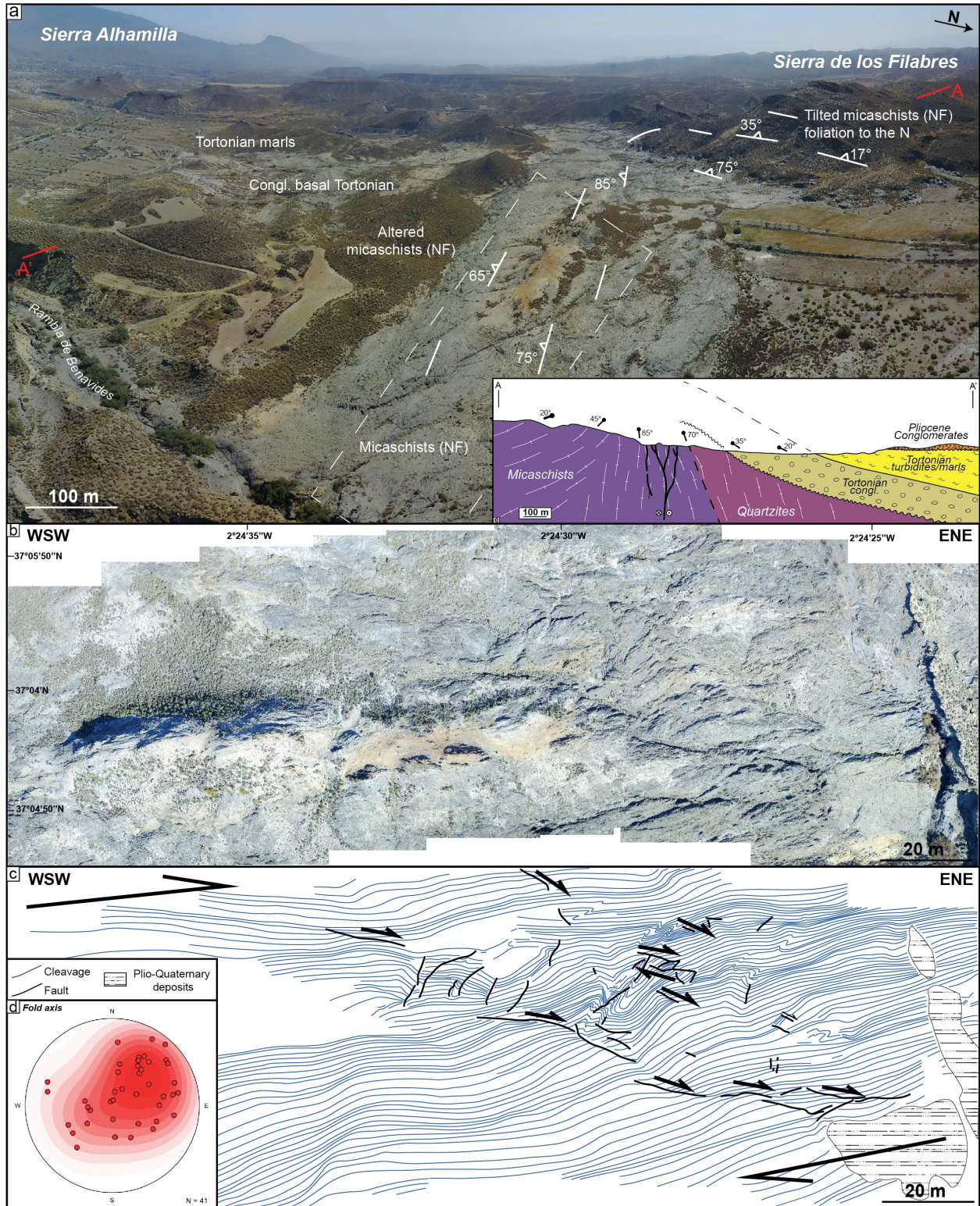
392
393 **Figure 10** : (**a**) Drone view taken in the SSW direction of the southern flank of the Sierra de los Filabres at the contact
394 with the Tabernas basin (see Figure 5 for location). Local folding of the micaschist is apparent in the right where the
395 foliation is striking NNE-SSW and is dipping ~25°E whereas it is vertical and striking SW-NE in the center of the
396 studied area forming paleosurface. Local cross section highlights the unconformable contact between the Tortonian
397 conglomerates and overlying on the basement. (**b**) High-resolution drone images of the paleosurface and (**c**) line-

398 drawing of the foliation revealing secondary folding (see (**d**) stereoplot of fold axes inclined to the NE) and dextral
399 shear zones. Coordinates 37.082777°N/-2.410544°E.
400

401

402
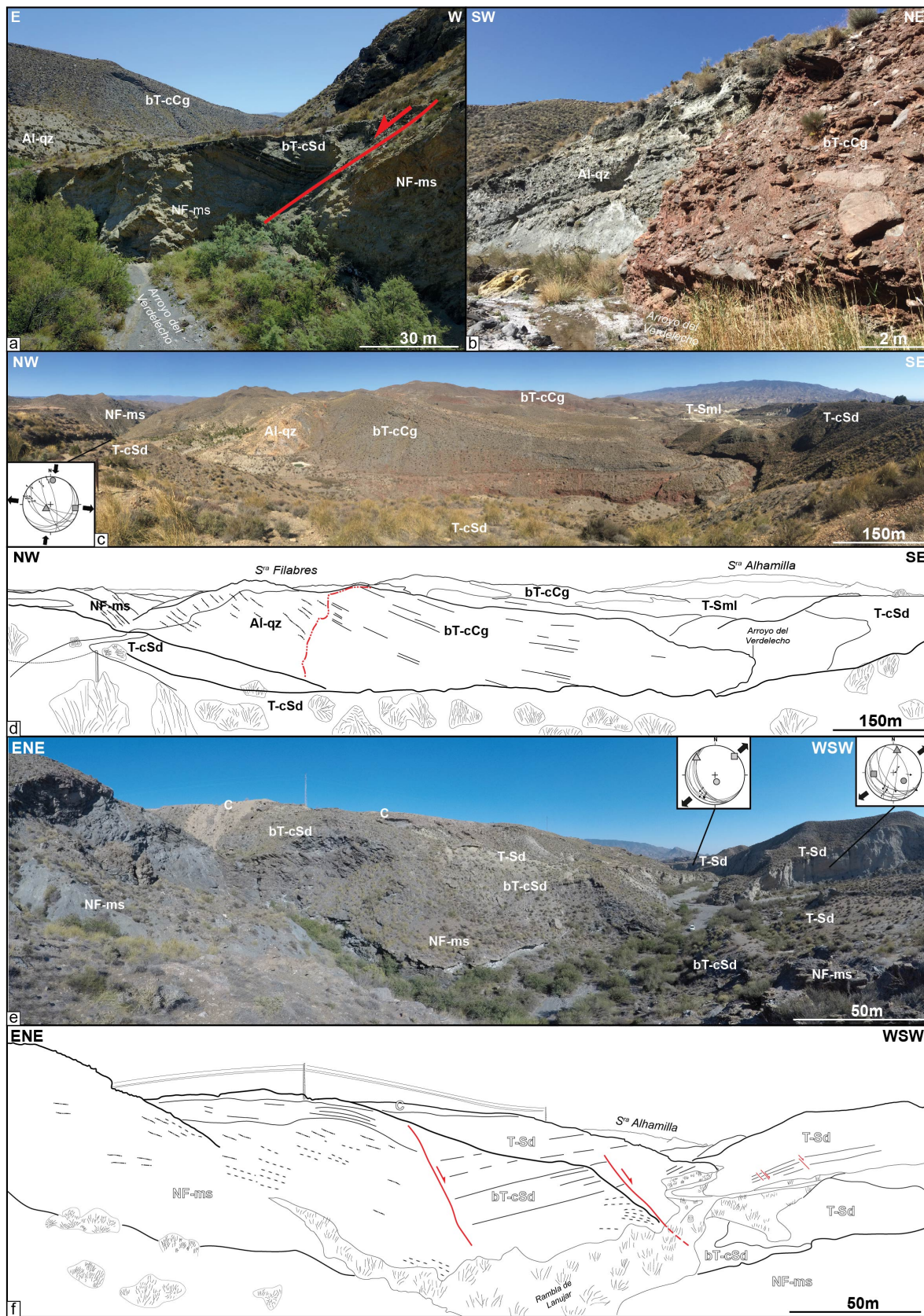
404 **Figure 11** : (**a**) Field photographs of a NW-SE normal fault at the contact between the Nevado-Filabride micaschists
405 (footwall) and Tortonian sediments (hanginwall). (**b**) Stratigraphic contact between grey and red basal Tortonian
406 continental conglomerates. These thick Tortonian series rest conformably on the Alpjuarride complex (**c**, **d**).
407 Coordinates 37.059507°N/-2.478386°E. (**e, f**) NW-SE normal faults cutting across the NF micaschists basement.
408 These faults that also affetc the early Tortonian deposits are sealed by late Tortonian deposits and are therefore syn-
409 depositional. See Figure 5 for location. Al-qz: Alpujarride quartzites; NF-ms: Nevado-Filabride micaschists; bT-cCg:
410 basal Tortonian continental Conglomerates; bT-cSd: basal Tortonian continental Sandstones; T-cSd: Tortonian coarse
411 Sandstones; T-Sd: Tortonian Sandstones; T-Sml: Tortonian Sandstones-marls; C: calcretes. Coordinates
412 37.061279°N/-2.490309°E. Paleostress orientations are in Table S1.

414 Both fault slip data and our own observations argue for a regional pre-Tortonian and syn-early Tortonian NNE-SSW
415 directed extension. This direction of extension is also found associated with less well-developed strike-slip regimes
416 (**Fig. 8**). It is consistent with the D1-D2 phase of brittle deformation found in HOB (Augier et al., 2013). The fact that
417 extension and strike-slip regimes occurred synchronously, or overlap rapidly in time, supports the view that they
418 reflect the same large-scale tectonic setting. The reason why strike-slip faulting is less apparent in the field than
419 expected in models in **Fig. 3** is likely to reflect the fact that oblique extension is not fully partitioned between normal
420 and strike-slip components and is actually distributed along oblique structures. Moreover, where strike-slip faults are
421 found they are associated with narrow basins or near the contact betwen the cover and basement but not in the center
422 of HOB or TB. The NNE-SSW to NW-SE faults appear to postdate the deposition of the early Tortonian red
423 conglomerates and is synchronous with the deposition of marine Tortonian series (**Fig. 12**). These normal faults
424 currently form half-graben filled with Plio-Quaternary deposits (Guadix, Baza, Alhabia) and are active today. But the
425 importance of extension-related brittle deformation over brittle compression decreases eastwards. Indeed, a late brittle
426 compressional event oriented roughly N-S is described in the literature as a D3 brittle event (e.g. in HOB) associated
427 with reverse and strike-slip faults (Augier et al., 2013). The post-late Tortonian shortening is seen responsible for fold
428 amplification and reverse faulting on the northern limb of Sierra de Alhamilla and Sierra de los Filabres, and locally
429 in the eastern part of the HOB near the termination of left-lateral strike-slip faulting evolution of the Alhama de Murcia
430 fault (**Fig. 8**).
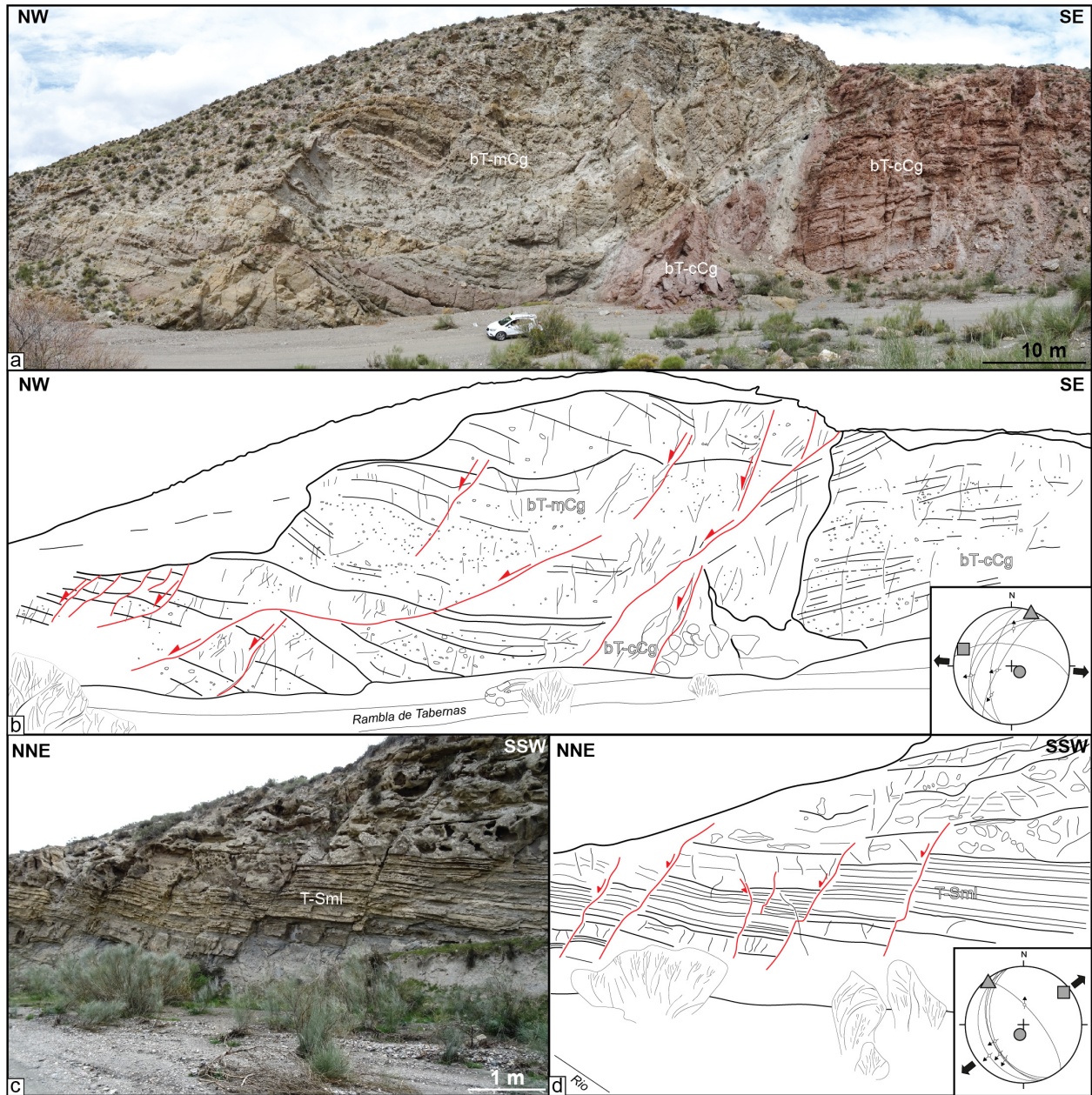
431

432 **Figure 12**: (**a, b**) N-S to NNE-SSW-oriented normal to dextral faults affecting the basal Tortonian continental
433 conglomerates (bT-cCg) and marine conglomerates (bT-mCg) (Rambla de Tabernas). They form a long and tight E-
434 W anticlinal crosses the Tabernas basin (see Figure 5 for location). (**c, d**) Several normal faults observed in Tortonian
435 sandstones and marls (T-Sml). They are mostly oriented NNW-SSE. Coordinates 37.041648°N/-2.399318°E.
436 Paleostress orientations are in Table S1.

437 **5. N-S crustal-scale section across the oblique/transform margin of Alboran basin**

438 To examine further the structural relationships between extension and strike-slip faulting across the Alboran margin,

439 we explore 2D multichannel seismic lines acquired during the MARSIBAL 1-06 cruise (Comas and MARSIBAL1-

440 06 Scientific Party, 2007) and ESCI cruises (Comas et al., 1995) across the Eastern Alboran basin (EAB). The studied

441 seismic dataset consists of ~300 km and are deep-penetration multichannel seismic reflection studies (12 s two-way

442 travel time - TWTT). Here, we study two lines namely MSB08 and MSB07 (see location in **Fig. 1**). For stratigraphic

and structural correlations between the studied seismic lines, we used the Andalucia-A1 well (**Fig. 6a**) and results
from ODP 977 and 978 legs (see location in **Fig. 1**). MSB08 is striking N70°E, slightly oblique to the shoreline. It is
close, and runs parallel, to TM08 line of Gómez de la Peña et al. (2018). It is calibrated by Andalucia-A1 well and
ESCI-Alb1 line (Comas et al., 1995). Line MSB07 stretches in the N-S direction between the EAB in Spain and SAB
to the north of Morocco parallel to line TM09 (Gómez de la Peña et al., 2018) and crosscusts line ESCI Alb2b
presented in Comas et al. (1995) and Booth-Rea et al. (2007) (**Fig. 1**).

5.1 Offshore structures and stratigraphic architecture

The Carboneras Fault is well imaged north of MSB07 (**Fig. 13**). It forms a negative crustal-scale flower structure
related to left-lateral strike-slip faulting that involves a Moho depth variation between 12 s to 9-8 s TWT after Gómez
de la Peña et al. (2018). It separates a thin continental crust to the North (25-20 km; **Fig. 2**), from the magmatic calc-
alkaline arc crust of the EAB with a thickness of 18 km in the south (Booth-Rea et al., 2007, 2018; Gómez de la Peña
et al., 2018, 2020a).
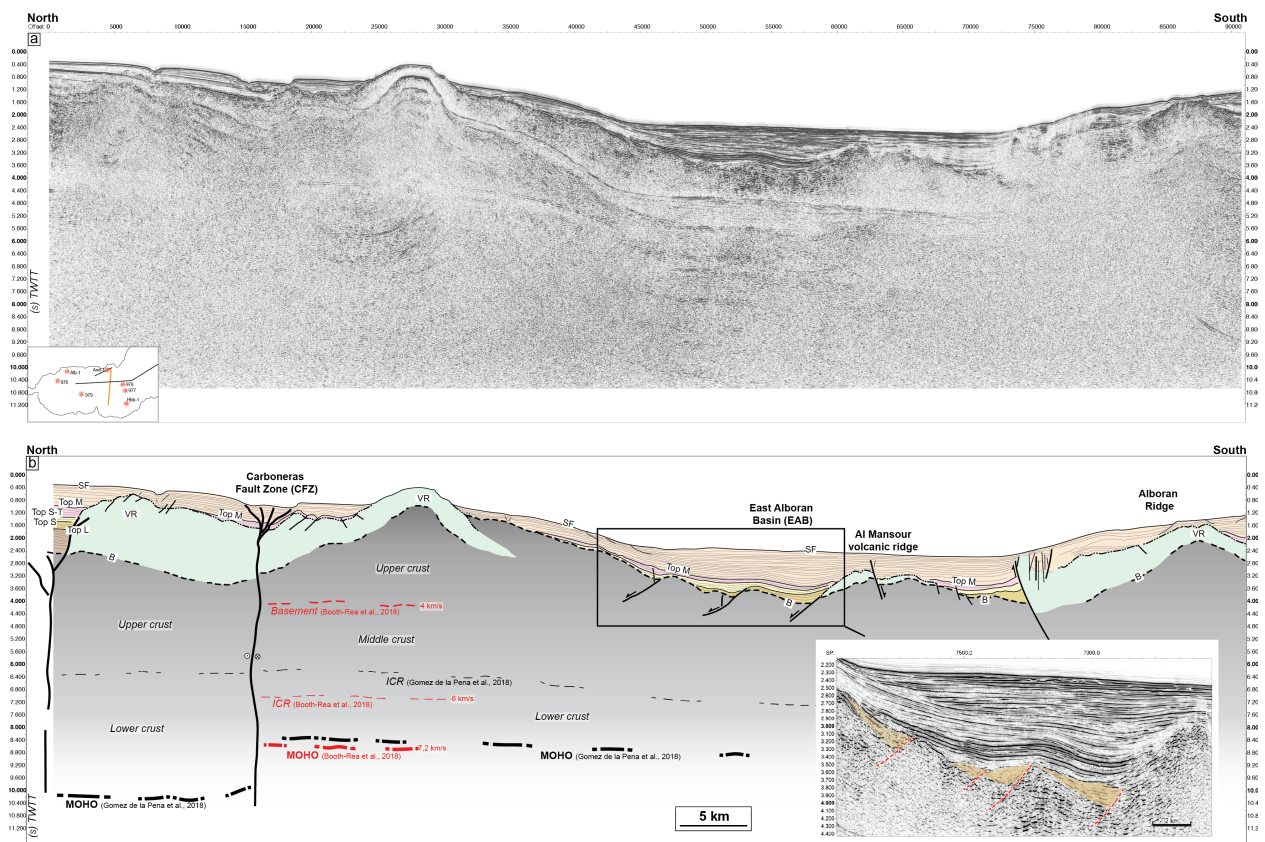
Figure 13 : Seismic reflection line MSB07 (location on **Fig. 1**). Discontinuous intracrustal reflectors (ICR) imaged
between 3 and 6.5 s TWT, have been interpreted as mylonitic zones within the metamorphic basement (Carbonell et
al., 1998; García-Dueñas et al., 1994; Gómez de la Peña et al., 2018). VR: Volcanic Ridge; B: Acoustic basement;
Top L : Top Langian; Top S: Top Serravallian; Top S-T: top Serravallian-Tortonian; Top M: Top Messinian; SF:
Seafloor.

464

465

466 Reflection seismic data (**Figs. 13, 14, 15**) collectively show a stratified crust, corresponding to the sediment cover,

467 down to 2.4-4 s TWT, which outlines the acoustic basement with high reflectivity (B). Locally, the top basement

468 reflector coincides with erosional palaeo-relief or high angle normal faults bounding basement highs. These faults are

469 oriented mostly NW-SE to NE-SW and cut across the basement. We recognized on seismic images magmatic additions

470 in the continental crust that are shaped by volcanic edifices exposed on the seafloor (e.g. Chella Bank) or slightly

471 buried (Alboran Ridge) outlined by symmetric downlaps and onlaps of sediments. These constructions form

472 topographic highs such as the Chella Bank on the MSB08 line (**Fig. 14**), the Alboran Ridge on the MSB07 line (**Fig.**

473 **13**) and the Maimonides Ridge on the ESCI-Alb2b line (**Fig. 15**). All the reflectors corresponding to layers as old as

474 Tortonian are onlapping against the volcanic ridges confirming that the volcanic activity occurred during the middle

475 to late Miocene times, which is shown by Duggen et al. (2008). Some reflectors up to the top Messinian (top M) onlap

476 onto the volcanic ridges probably as a result of Pliocene uplift.

477 The stratigraphy offshore, on the continental crustal domain, is defined by the recognition of five seismic stratigraphic

478 units in Andalucía-A1 well (Jurado and Comas, 1992) labeled I-V from top to base (**Figs 6** and **16**) and separated by

479 unconformities. The seismostratigraphic units I to V vary in thickness **(Fig. 16)** and their architecture is conditioned

480 by the occurrence of basement highs and crustal-scale faults.

481 Below the Miocene sedimentary filling, Andalucia-A1 well reveals ~190m of phyllitic and quartzitic meta-sediments

482 (2.4 to 4 s TWT below the Alboran basin, **Figs. 13** and **14**) topped by Langhian to Tortonian marls (top at ~1.6 to 3.4

483 s TWT below the Alboran basin) interbedded with Tortonian-Messinian tuffs and basaltic lavas. These units have

484 been correlated in the magmatic arc crust of EAB after Gómez de la Peña et al. (2020b). The older deposits (Unit V)

485 Langhian-Serravallian in age, consist of clays and marls with intercalated sands and volcano-clastic deposits. The

486 seismic facies of this Unit V is made of moderate amplitude and low frequency discontinuous reflections packages

487 (Figure **16**), and is only present in the Northern Alboran Basin. They are correlated with volcanic series in the EAB

488 (vY3) (Gómez de la Peña et al., 2020b). They pass upward into Serravallian sand-silty clay turbidite (Unit IV) possibly

489 correlated with volcanic series in EAB (vY2 after Gómez de la Peña et al., 2020b). This unit exhibiting low to moderate

490 amplitude, moderate frequency drawing continuous sheeted to disrupted reflectors, is unconformably overlying Unit

491 V and locally onlaps onto the basement. Thickness of Unit IV remains rather thin in the North and East Alboran Basin.

492 It can't be properly identified in the South Balearic Basin, east of the Maimonides volcanic ridge (**Fig. 15**). The Unit

493 III dated from late Serravallian to late Tortonian is represented by sandstones interbedded with volcano-clastic levels

494 whih correlates in EAB with volanics vY1 unit. Unit III contains internal reflections characterized by low to moderate

495 amplitude, moderate frequency continuous sheeted reflectors. Its thickness remains relatively constant from the NAB

496 to the EAB, and is identified beneath the Messinian Unit II in the South Balearic Basin. Unit II corresponds to the

497 Messinian evaporite, carbonate, volcanic, and volcaniclastic deposits interbedded with fine-grained sediments and is

498 equivalent to unit III of Gómez de la Peña et al. (2020b) in EAB. Seismic facies of Unit II is marked in the Alboran

499 domain by lower amplitudes and lower frequency reflectors. In ESCI-Alb2b line, Unit II increases drastically east of

500 the Maimonides ridge, which delimits the western boundary of the salt deposits in the Western Mediterranean basin

during the Messinian Salinity Crisis (Haq et al., 2020). Unit II is topped by Unit I made of Pliocene to Quaternary clays and sanstones, which are correlated with units II and I in EAB (Gómez de la Peña et al., 2020b). Unit I is marked by thinly bedded, mostly parallel, high-frequency and low amplitudes reflectors (**Fig. 15**). Its thickness fluctuates in response to sedimentary processes (Juan et al., 2016).

Along line MSB08 (**Fig. 14**) the Langhian-Serravallian (Unit V) is maximum 1600 m-thick (using a P-wave velocity of 3.2 km/s calculated within Andalucia-A1 well). In EAB, south of Carboneras Fault Zone, the total thickness of Unit V is only ~300 m on MSB07 (**Fig. 13**) and is absent in ESCI-Alb2b (**Fig. 15**). The Serravallian-Tortonian (Unit IV-III) interval shows only very limited sediment accumulation (~300 m) except near the NW-SE oriented normal faults where growth geometries are visible. These normal faults are sealed by the Tortonian-Messinian deposits, indicating a syn-sedimentary faulting during the middle Miocene (**Fig. 13**). With respect to onshore observations this sedimentary infill is more continuous and is also much thinner compared to TB and HOB where they are represented by thick conglomerates and marls/turbidites (> 1km) (**Fig. 7**), and they are eroded or not deposited along the axes of the metamorphic domes. The Messinian deposits (Unit II) are ~150-350 m-thick north of CF (MSB07-08 ; **Figs. 13, 14**) and increase to about 1200 m eastward in the eastern EAB (ESCI-Alb2b ; **Fig. 15**), and in Algero-Balearic basin (Gómez de la Peña et al., 2020b). The top Messinian reflector is topped by thick horizontal sedimentary strata, with a maximum thickness of 1.2 s TWT (~2.4 km assuming a velocity of 2 km/s) on line MSB07, suggesting an important channel system during the Pliocene.

The Pliocene-to-Quaternary series are poorly deformed except in the vicinity of CF and near the Alboran Ridge where this is associated with south-dipping reverse fault (**Fig. 13**). This late and still active compressional tectonics is revealed by the overthrusting of the SAB over the south margin of the EAB (e.g. Martínez-García et al., 2011).
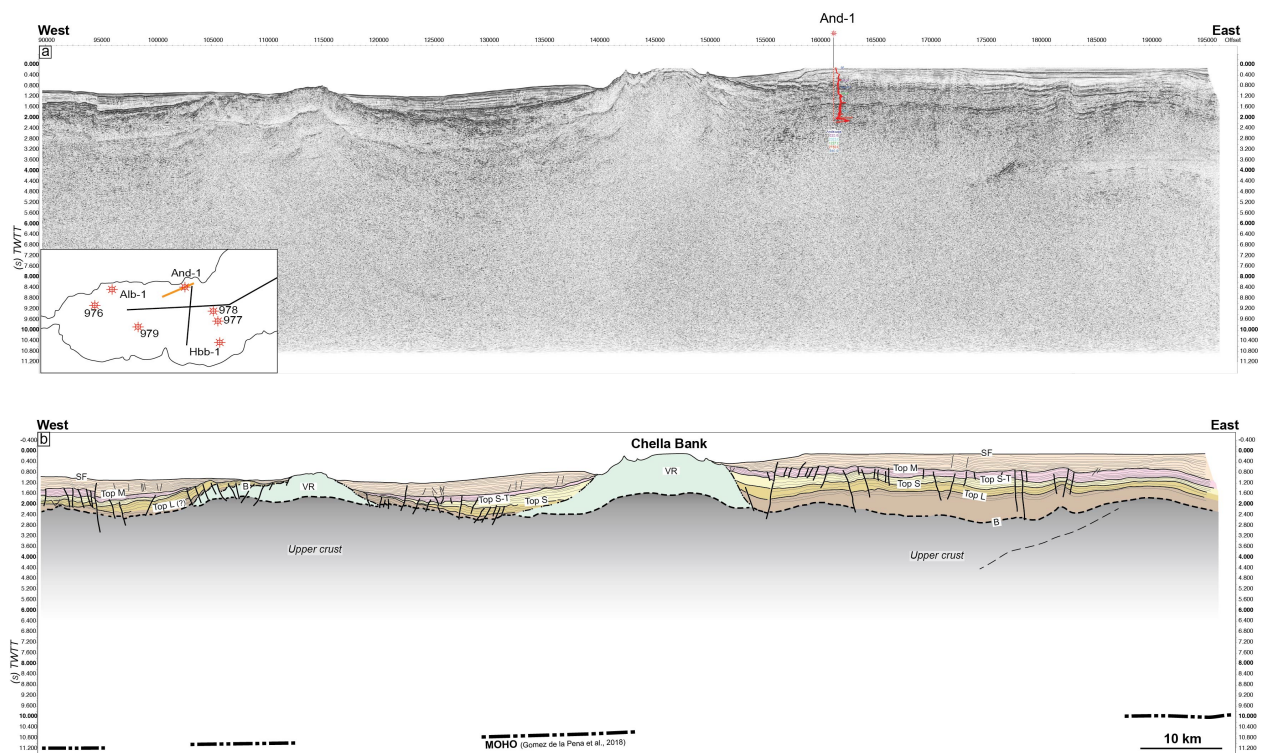
523 **Figure 14** : Seismic reflection line MSB08 (see location on **Fig. 1**). See Figure 13 for abbreviations. See also Figure
524 S3 showing a zoom on the main seismic facies recognized in Andalucia-A1 well.
525
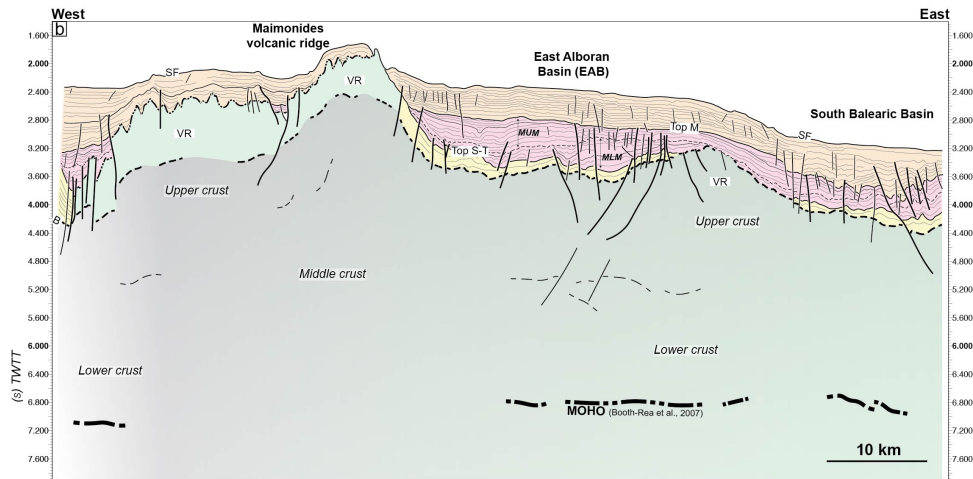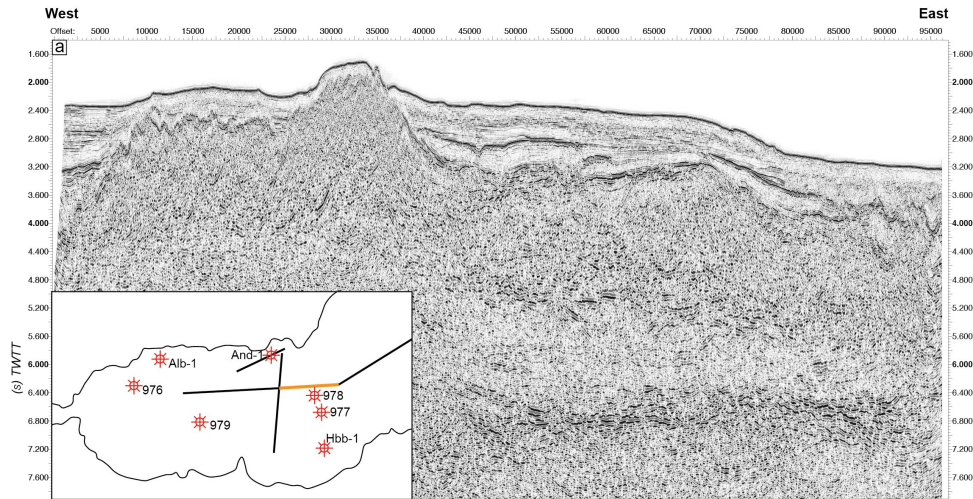
526
527 **Figure 15**. (**a, b**) Seismic reflection line ESCI-Alb2b and intepretation (see Figure 1 for location). Seismic units are
528 correlated with those defined by Booth-Rea et al. (2007). See Figure 13 for abbreviations.
529

530
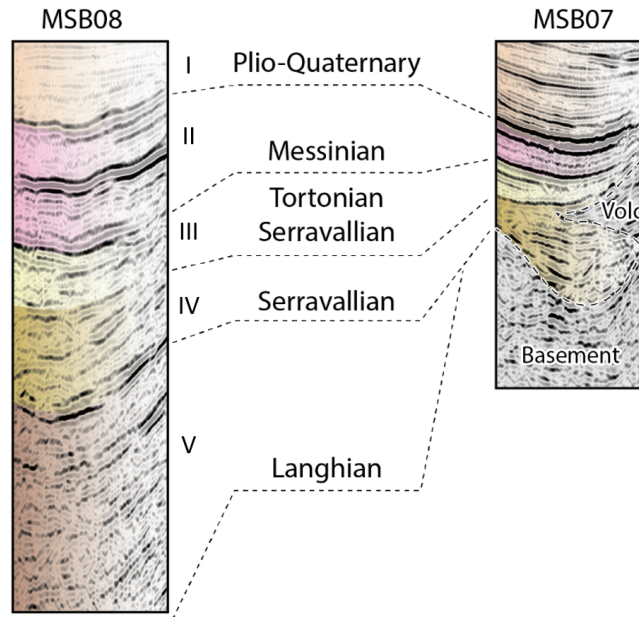
531

532 **Figure 16** : Seismic facies of units I to V seen through seismic lines MSB08 close to the shoreline and the line
533 MSB07, located deeper in the East Alboran Basin.

534 **5.2 N-S crustal cross-section of the Alboran margin accounting for strike-slip faulting**

535 Based on subsurface constraints and field data, we present in **Figure 17** a crustal-scale section across the rifted margin,

536 from the Sierra de las Estancias and Huercal-Overa basin (HOB) to the Alboran ridge that represents the inverted

537 southern margin of the EAB. The proximal margin, where the crust is 30-35 km-thick, is defined to the North by the

538 transition between the south Iberia margin, and the metamorphic domain of the Alboran basement exposed in the

539 Sierra de las Estancias. This continental domain preserves part of the crustal thickness acquired during former Betic

540 orogenic phase that has been little involved in crustal thinning. The onset of crustal thinning to the south coincides

541 with the position of the lithospheric tear fault documented by seismology (**Fig. 4**; Mancilla et al., 2015a) and is

542 recorded by the formation of asymmetric basins of the HOB and TB, shaping the upper neck domain. Orthogonal and

543 oblique extension in this domain is accommodated by normal and strike-slip faulting during the Tortonian. From the

544 Sierra de los Filabres to the south, the thickness of the continental crust reduces to 25 km in the Tabernas basin along

545 the Alpujarras strike-slip fault zone and below the Sierra Alhamilla (**Fig. 17**). The Nijar basin depicts the transition

546 towards offshore distal domains where the continental crust reaches a thickness of 20 km. The Tortonian and

547 Messinian marine sediments are also thicker. It is worth noting that a number of volcanic bodies offshore (e.g. Chella

548 Bank on MSB08) accompany crustal thinning of the continental crust. The Carboneras Fault (CF) brings crusts with

549 different thicknesses and composition into contact. South of CF, the crustal thickness of the EAB is 18 km and seismic

550 velocities, especially the occurrence of a high-Vp lower crust, has been considered to indicate the EAB is floored by

551 a magmatic arc crust (Gómez de la Peña et al., 2018; 2020), formed in a supra-subduction context above the subducting

552 Alboran slab (Booth-Rea et al., 2018). The crustal thickness of the EAB is compatible with crustal thinning of the

553 continental margin, and the occurrence of NW-SE-trending faults also recognized onshore despite being slightly older

554 (Serravalian-Tortonian) suggest that the EAB formed under the same back-arc extension setting, relative to westward

555 slab retreat as the whole Alboran margin did. Thus, the magmatic arc crust of the EAB could represent voluminous
556 magmatic intrusions (e.g. Al Mansour dacite, Alboran Ridge rhyolite dated to ca. 9 Ma; Duggen et al., 2004; Tendero-
557 Salmerón et al., 2022; **Fig 17**) formed on the distal rifted margin of Alboran. The investigation of the causes of calc-
558 alkaline magmatism is beyond the scope of this study, but we suspect it reflects post-subduction arc magmatism
559 induced by remelting, during extension and delamination, of a metasomatized wedge of mantle lithosphere formed
560 during a previous subduction event (e.g. Richards, 2009). The fact that calc-alkaline magmatism around 10 Ma that is
561 10 to 5 myrs after the onset of upper plate extension in the Betic-Alboran region supports this view. Note that in
562 contrast to Gómez de la Peña et al. (2020) and Booth-Rea et al. (2018) we implicitly assume the magmatic arc crust
563 of EAB is not a newly formed crust but rather represents a thinned continental crust later intruded by calc-alkaline
564 magmas. Different crustal domains are expected across a rifted margin that has involved variable amount and types
565 of mantle-derived magmatism, especially if delamination/subduction occurred during extension. The observation of
566 contrasting types of crustal domains now juxtaposed in the NS direction is also related to the fact that extension is
567 oriented perpendicular to the section.
568 Crustal shortening in **Figure 17** is distributed across north-vergent reverse faults below the Alboran Ridge, on the
569 northern limb of Sierra de Alhamilla, and CF strike-slip fault zone.
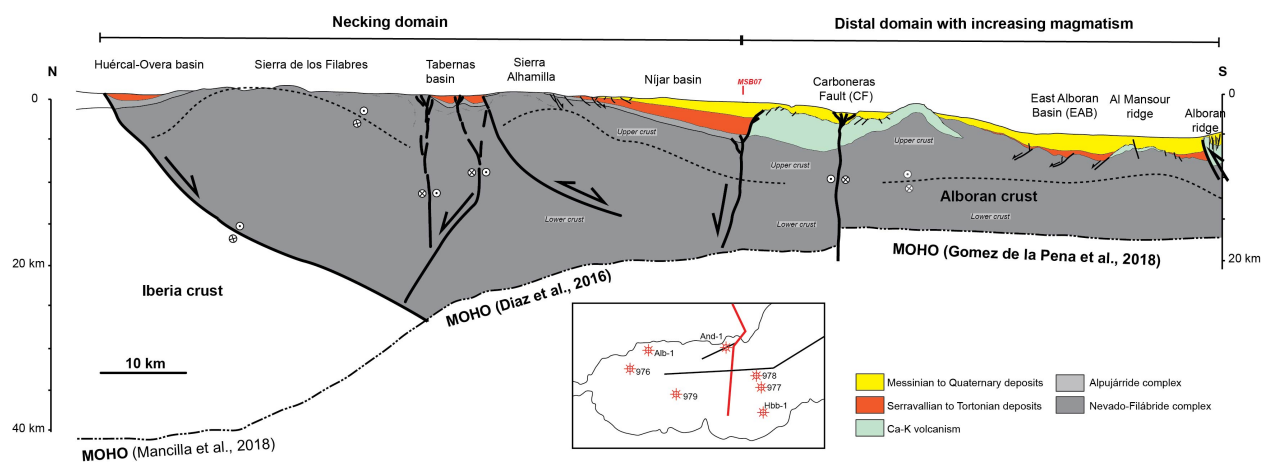
570

571 **Figure 17**. Crustal-scale cross section of the Alboran margin in the eastern Betics interpreted based on onshore and
572 offshore contraints presented in the text. Note that in the necking domain the extension of faults downwards to
573 Moho depths is not imaged on the seismics and therefore largely inspired by inferences from 3D numerical models
574 (see Fig. 3).
575
576

6. Implications

The question of whether the Miocene tectonic evolution of the Betics reflects crustal thinning associated with oblique back-arc rifting as suggested from present-day strain patterns is unclear in the literature. We found based on a comparison between numerical models and basin analyses, fault kinematics and structure of the margin in the eastern Betics compelling evidences that crustal thinning was controlled by oblique extension. Oblique rifting operated since at least the middle Miocene in relation with Alboran slab retreat below the Alboran basin and is kinematically associated with slab tearing and delamination below the central and eastern Betics.

One of the most striking tectonic feature of the Alboran margin (**Fig. 17**) is the abrupt N-S crustal thinning oblique to the direction of slab rollback. The history of sediment infill and rates of subsidence in intramontane basins (**Figs. 6 and 7**) combined with the analyses of fault slip data (**Fig. 8**), and structural data offshore (**Fig. 13**), confirm that brittle extension oriented from N20°E to EW occurred during an interval spanning from the Serravallian-early Tortonian to the late Tortonian (14-8 Ma) (**Fig. 18**). This extension is found associated with both normal and strike-slip regimes. Field tectonic data reveal that N20°E extension is more represented in HOB while the ENE-WSW to EW extension is found related with the evolution of the Almanzora fault zone, Alpujarras fault zone and Tabernas basin flanking the metamorphic domes (**Table S1**). There are additional evidence that EW-directed dextral strike-slip faulting occurred during the Tortonian to the South and West of the HOB. These large-scale transfer fault zones positioned on the slab edge accommodate the differential westward extension that are later cut by Tortonian NW-SE faults. These second set of faults is also observed in the magmatic crust of the EAB offshore but seismic data indicate they are Serravallian-Tortonian in age and therefore older than those identified onshore. We suggest that NW-SE normal faulting could have initiated in the EAB then migrated towards the necking domain as slab retreat progressed and the width of the region affected by crustal thinning widened (**Fig. 18**). Subsidence during the Serravallian-Tortonian appears to have been lower in the EAB compared to intramontane basins onshore. This suggests that the isostatic effect of crustal thinning was compensated by a thermal anomaly in the mantle, heralding the Ca-K magmatism at 11-7 Ma (Duggen et al., 2004, 2008).
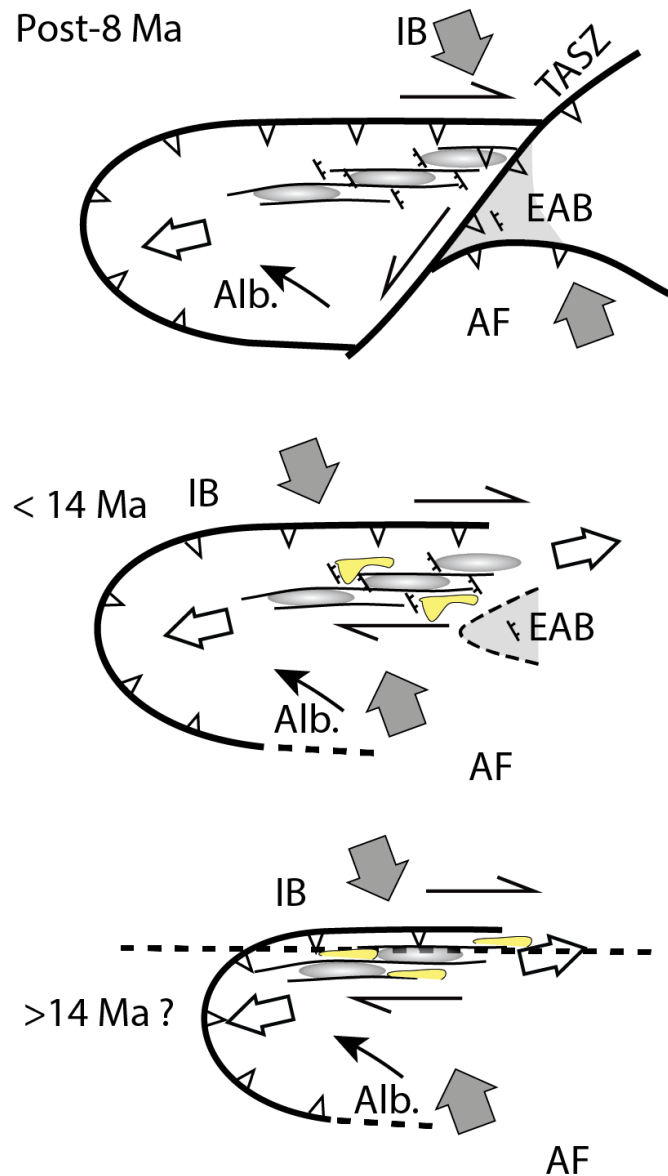
602

603 **Figure 18**: Tectonic model of the evolution of the northern margin of the Alboran Rift. Large grey and white double
604 arrows depict shortening, which is parallel to the AF/IB convergence, and the highly oblique extension, respectively.
605 The thin black arrows show the motion of Alboran relative to Iberia (IB) taken from Figure 4. Half arrows depict
606 distributed strike-slip faulting in the Betics. NW-SE directed normal fault and strike-slip basins (yellow) are
607 consistent with the oblique extension. Grey-shaded ellipses represent the metamorphic domes. TASZ : simplified
608 representation of the Trans-Alboran Shear Zone. We also indicated EAB which mostly formed ca. 9 Ma (Duggen et
609 al., 2004; Booth-Rea et al., 2018).

610

611 Several key tectonic features found in the eastern Betics are predicted by 3D models of oblique extension (**Figure 3**).

612 They include E-W trending normal faults that are prevalent on the upper neck domain (i.e. Sierra de las Estancias and

613 HOB), and E-W strike-slip faults (Almanzora and Alpujarras fault zones). NW-SE normal faults are associated with

614 more distal domains on the continental margin where crustal thinning is the highest offshore, south of Nijar basin, and
615 in the EAB.

616 Tectonic inversion seems, in contrast, to have been increasingly more important when approaching the Carboneras
617 and Palomares strike-slip faults in the East since the late Tortonian.

618 Ductile thinning associated with the formation of metamorphic domes and exhumation of HP rocks is dated to 23 to
619 16 Ma (Platt et al., 2003; Booth-Rea et al., 2015). This provides time constraint for the beginning of oblique extension
620 and westward slab rollback. Deformation at the future location of the tear fault was probably initially diffuse and
621 resulted in an immature oblique rift system in the South, combined with thrusting in the external zones to the North
622 (**Figure 18**). In the Serravallian (14-13 Ma), accompanying slab steepening, localization of slab tearing, and
623 propagation of thrusting in external zones, oblique extension spread over the whole central Betics. At this time,
624 metamorphic domes exhumed to upper crustal levels (e.g. Vázquez et al., 2011) and recorded the transition from
625 ductile shearing to brittle faulting (**Figure 18**). Brittle E-W-directed stretching and dextral transcurrent deformation
626 formed at this time. The late/post-Tortonian times (from 10-8 Ma) marks a change in the tectonic evolution of the
627 Betics and Alboran domain possibly related to the onset of slab detachment in the eastern Betics (van Hinsbergen et
628 al., 2014; Do Couto et al., 2014; Mancilla et al., 2015a; Martínez-García et al., 2017; d'Acremont et al., 2020; García-
629 Castellanos and Villaseñor, 2011; Spakman et al., 2018). This event is synchronous with the indendation by the
630 magmatic arc crust of the EAB in the Águilas Arc (Ercilla et al., 2022), amplification of the metamorphic domes in
631 the vicinity of the EBSZ (e.g. Alhamilla), transition from Ca-K in EAB to more alkaline magmatism in eastern Betics,
632 and at the regional scale with exhumation in northern Iberia (Rat et al., 2022) and N-S shortening in northern Africa
633 (Jolivet al., 2021a) (**Figure 18**).

634 In this model, ductile stretching and ductile detachment associated with the development of the domes are the
635 expression of oblique E-W extension. It provides a coherent scheme linking the formation of EW-directed basins in
636 the brittle field associated with strike-slip faulting, and NW-SE/NNW-SSE sedimentary basins (Guadix, Baza,
637 Alhabia) formed in transtension during the Tortonian. As such, the oblique extension is closely associated with STEP
638 faulting required by westward slab rollback. The oblique rifting model we propose explain the formation of the
639 metamorphic domes and intermontane basins and provides insight into crustal deformation, which is broadly
640 consistent with the geodynamic models of slab rollback and tearing since 20 Ma that have been previously proposed
641 for Alboran (Chertova et al., 2014; Spakman et al., 2018). In the latter models, however, the ENE-WSW extension in
642 the central-eastern Betics is related to differential absolute motions between Iberia and the slab decoupled from Iberia
643 by slab tearing. In our scenario, oblique extension is entirely related to westward lateral rollback. It can not be
644 excluded, however, that the effect of mantle-derived slab dragging increased during the late extensional stage, from
645 14-13 Ma, when slab tearing localized.

646 Mid-Miocene high-pressure metamorphism documented in the central Betics (e.g. Platt et al., 2013) was synchronous
647 with slab steepening and subduction that was under way during oblique back-arc extension (**Figure 18**). The case of
648 exhumation of high-pressure rocks in oblique convergence setting associated with near-parallel orogen extension is
649 also documented in other active orogen like Taiwan (Conand et al., 2020).

650 This highly oblique northern Alboran margin differs from typical transform fault margin such as those associated with
651 the Altantic ocean because it accommodates variations in intra-plate extensional movements, triggered by slab roll-
652 back, not variations in spreading rates. Strike-slip faults may have originated as low-angle normal faults which were
653 later reactivated as thrusts during margin inversion. Similar observations, including metamorphism, strike-slip
654 faulting, high geothermal gradients and volcanism has been made in Seram, north of the Banda Arc, which represents
655 another example of extremely thinned crust formed perpendicular to the direction of the slab rollback (Pownall et al.,
656 2013). Such a narrow rifted margin associated with lithospheric STEP fault defines a class of oblique margin that is
657 expected to be hardly preserved in the geological record due the transient nature of retreating subduction systems.
658
659

660 **Data availability**.This study is based on data compilation. Data used in this study can be found in the appropriate
661 references. Paleostress tensors obtained by the inversion of fault slip data are available online in the Supplement.
662
663 **Supplement**.The supplement related to this article is available on-line at:
664
665 **Competing interests**.The authors declare that they have no conflictof interest.

666 **Authors contribution**
667 ML and FM, conceptualize, prepared figures and tables, compiled and interpreted field structural data and wrote the
668 paper. DC provided and interpreted the seismic lines, reviewed the text and contributed to the writing. AJ carefully
669 exmined the implementation of his numerical results and reviewed the text. EM, SC and VM, supervised and
670 coordinate the different project tasks and reviewed the text.

671 **Acknowledgments**
672 Víctor Tendero Salmerón, Guillermo Booth-Rea, and an anonymous reviewers are warmly thanked for their comments
673 that greatly improved the manuscript. The stereogram results were obtained using Win-Tensor, a software developed
674 by Dr. Damien Delvaux, Royal Museum for Central Africa, Tervuren, Belgium (Delvaux and Sperner, 2003). The
675 processed seismic data were interpreted using Kingdom IHS Suite© software. This research benefited from
676 discussions and support of OROGEN project, an academic-industry research consortium between TOTAL, CNRS and
677 BRGM.

678
679

680   **References**

681   Angrand, P., Mouthereau, F., 2021. Evolution of the Alpine orogenic belts in the Western Mediterranean region as
682   resolved by the kinematics of the Europe-Africa diffuse plate boundary. Bsgf - Earth Sci Bulletin.
683   https://doi.org/10.1051/bsgf/2021031
684   Argus, D.F., Gordon, R.G., DeMets, C., 2011. Geologically current motion of 56 plates relative to the no-net-
685   rotation reference frame. Geochemistry, Geophysics, Geosystems 12. https://doi.org/10.1029/2011gc003751
686   Augier, R., 2004. Evolution tardi-orogénique des Cordillères Betiques (Espagne) : apports d'une étude integrée 1
687   vol., [II]-400 p.
688   Augier, R, Agard, P., Monié, P., Jolivet, L., Robin, C., Booth-Rea, G., 2005. Exhumation, doming and slab retreat in
689   the Betic Cordillera (SE Spain): in situ40Ar/39Ar ages and P–T–d–t paths for the Nevado-Filabride complex.
690   Journal of Metamorphic Geology 23, 357–381. https://doi.org/10.1111/j.1525-1314.2005.00581.x
691   Augier, R., Booth-Rea, G., Agard, P., Martínez-Martínez, J.M., Jolivet, L., Azañón, J.M., 2005a. Exhumation
692   constraints for the lower Nevado-Filabride Complex (Betic Cordillera, SE Spain): a Raman thermometry and
693   Tweequ multiequilibrium thermobarometry approach. Bulletin de la Societe Geologique de France 176, 403–
694   416. https://doi.org/10.2113/176.5.403
695   Augier, R., Jolivet, L., couto, D.D., Negro, F., 2013. From ductile to brittle, late- to post-orogenic evolution of the
696   Betic Cordillera: Structural insights from the northeastern Internal zones. Bulletin De La Société Géologique De
697   France 184, 405–425. https://doi.org/10.2113/gssgfbull.184.4-5.405
698   Augier, R., Jolivet, L., Robin, C., 2005b. Late Orogenic doming in the eastern Betic Cordilleras: Final exhumation
699   of the Nevado-Filabride complex and its relation to basin genesis. Tectonics 24, n/a-n/a.
700   https://doi.org/10.1029/2004tc001687
701   Badji, R., Charvis, P., Bracene, R., Galve, A., Badsi, M., Ribodetti, A., Benaissa, Z., Klingelhoefer, F., Medaouri,
702   M., Beslier, M.-O., 2014. Geophysical evidence for a transform margin offshore Western Algeria: a witness of a
703   subduction-transform edge propagator? Geophys J Int 200, 1029–1045. https://doi.org/10.1093/gji/ggu454
704   Barcos, L., Balanyá, J.C., Díaz-Azpiroz, M., Expósito, I., Jiménez-Bonilla, A., 2015. Kinematics of the Torcal Shear
705   Zone: Transpressional tectonics in a salient-recess transition at the northern Gibraltar Arc. Tectonophysics 663,
706   62–77. https://doi.org/10.1016/j.tecto.2015.05.002
707   Baudouy, L., Haughton, P.D.W., Walsh, J.J., 2021. Evolution of a Fault-Controlled, Deep-Water Sub-Basin,
708   Tabernas, SE Spain. Frontiers Earth Sci 9, 767286. https://doi.org/10.3389/feart.2021.767286.
709   Bessière, E., Jolivet, L., Augier, R., Scaillet, S., Précigout, J., Azañon, J.-M., Crespo-Blanc, A., Masini, E., Couto,
710   D.D., 2021. Lateral variations of pressure-temperature evolution in non-cylindrical orogens and 3-D subduction
711   dynamics: the Betic-Rif Cordillera example. Bsgf - Earth Sci Bulletin. https://doi.org/10.1051/bsgf/2021007
712   Bezada, M.J., Humphreys, E.D., Toomey, D.R., Harnafi, M., Dávila, J.M., Gallart, J., 2013. Evidence for slab
713   rollback in westernmost Mediterranean from improved upper mantle imaging. Earth and Planetary Science
714   Letters 368, 51–60. https://doi.org/10.1016/j.epsl.2013.02.024
715   Booth-Rea, G., Martínez-Martínez, J.M., Giaconia, F., 2015. Continental subduction, intracrustal shortening, and
716   coeval upper-crustal extension: P-T evolution of subducted south Iberian paleomargin metapelites (Betics, SE
717   Spain). Tectonophysics 663, 122–139. https://doi.org/10.1016/j.tecto.2015.08.036
718   Booth-Rea, G., Ranero, C.R., Grevemeyer, I., 2018. The Alboran volcanic-arc modulated the Messinian faunal
719   exchange and salinity crisis. Scientific reports 8, 13015. https://doi.org/10.1038/s41598-018-31307-7
720   Booth-Rea, G., Ranero, C.R., Martinez-Martinez, J.M., Grevemeyer, I., 2007. Crustal types and Tertiary tectonic
721   evolution of the Alborán sea, western Mediterranean. Geochemistry, Geophysics, Geosystems 8, n/a-n/a.
722   https://doi.org/10.1029/2007gc001639
723   Booth-Rea, G., Azañón, J.-M., Azor, A., García-Dueñas, V., 2004a. Influence of strike-slip fault segmentation on
724   drainage evolution and topography. A case study: the Palomares Fault Zone (southeastern Betics, Spain). J
725   Struct Geol 26, 1615–1632. https://doi.org/10.1016/j.jsg.2004.01.007
726   Booth-Rea, G., Azañón, J.M., García-Dueñas, V., 2004b. Extensional tectonics in the northeastern Betics (SE
727   Spain): case study of extension in a multilayered upper crust with contrasting rheologies. Journal of structural
728   geology 26, 2039–2058. https://doi.org/10.1016/j.jsg.2004.04.005
729   Borque, M.J., Alzola, A.S., Martin-Rojas, I., Alfaro, P., Molina, S., Cintas, S.R., Caderot, G.R., Lacy, C., Avilés,
730   M., Olmo, A.H., Tortosa, F.J.G., Estévez, A., Gil, A.J., 2019. How Much Nubia-Eurasia Convergence Is
731   Accommodated by the NE End of the Eastern Betic Shear Zone (SE Spain)? Constraints From GPS Velocities.
732   Tectonics 38, 271–1839. https://doi.org/10.1029/2018tc004970
733   Braga, J.C., Martín, J.M., Quesada, C., 2003. Patterns and average rates of late Neogene–Recent uplift of the Betic
734   Cordillera, SE Spain. Geomorphology 50, 3–26. https://doi.org/10.1016/s0169-555x(02)00205-2

735 Carbonell, R., Sallares, V., Pous, J., Dañobeitia, J.J., Queralt, P., Ledo, J.J., Dueñas, V.G., 1998. A multidisciplinary
736   geophysical study in the Betic chain (southern Iberia Peninsula). Tectonophysics 288, 137–152.
737   https://doi.org/10.1016/s0040-1951(97)00289-8
738 Clark, S.J.P., Dempster, T.J., 2009. The record of tectonic denudation and erosion in an emerging orogen: an apatite
739   fission-track study of the Sierra Nevada, southern Spain. Journal of the Geological Society 166, 87–100.
740   https://doi.org/10.1144/0016-76492008-041
741 Comas, M. C., J. J. Dañobeitia, J. Alvarez-Maron, and J. I. Soto (1995), Crustal reflections and structure in the
742   Alboran Basin. Preliminary results of the ESCI-Alboran survey, Rev. Soc. Geol. Esp., 8(4), 529 – 542.
743 Comas, M.C., García-Dueñas, V., Jurado, M.J., 1992. Neogene tectonic evolution of the Alboran Sea from MCS
744   data. Geo-mar Lett 12, 157–164. https://doi.org/10.1007/bf02084927
745 Comas, M., and MARSIBAL 1-06 Scientific Party (2007). Preliminary results of Marsibal 1-06 cruise in the
746   Alboran and western Algero-Balearic basins. Geophys. Res. Abst., 9, 10871.
747 Conand, C., Mouthereau, F., Ganne, J., Lin, A.T., Lahfid, A., Daudet, M., Mesalles, L., Giletycz, S., Bonzani, M.,
748   2020. Strain Partitioning and Exhumation in Oblique Taiwan Collision: Role of Rift Architecture and Plate
749   Kinematics. Tectonics 39, e2019TC005798. https://doi.org/10.1029/2019tc005798
750 Crespo-Blanc, A., Comas, M., Balanyá, J.C., 2016. Clues for a Tortonian reconstruction of the Gibraltar Arc:
751   Structural pattern, deformation diachronism and block rotations. Tectonophysics 683, 308–324.
752   https://doi.org/10.1016/j.tecto.2016.05.045
753 d'Acremont, E., Lafosse, M., Rabaute, A., Teurquety, G., Couto, D.D., Ercilla, G., Juan, C., Lépinay, B.M.,
754   Lafuerza, S., Galindo-Zaldivar, J., Estrada, F., Vazquez, J.T., Leroy, S., Poort, J., Ammar, A., Gorini, C., 2020.
755   Polyphase Tectonic Evolution of Fore-Arc Basin Related to STEP Fault as Revealed by Seismic Reflection Data
756   From the Alboran Sea (W-Mediterranean). Tectonics 39. https://doi.org/10.1029/2019tc005885
757 Dalziel, I.W.D., Lawver, L.A., Norton, I.O., Gahagan, L.M., 2013. The Scotia Arc: Genesis, Evolution, Global
758   Significance. Annu Rev Earth Pl Sc 41, 767–793. https://doi.org/10.1146/annurev-earth-050212-124155
759 Daudet, M., Mouthereau, F., Brichau, S., Crespo-Blanc, A., Gautheron, C., Angrand, P., 2020. Tectono-
760   Stratigraphic and Thermal Evolution of the Western Betic Flysch: Implications for the Geodynamics of South
761   Iberian Margin and Alboran Domain. Tectonics 39. https://doi.org/10.1029/2020tc006093
762 Dewey, J.F., 1988. Extensional collapse of orogens. Tectonics 7, 1123–1139.
763   https://doi.org/10.1029/tc007i006p01123
764 Dewey, J.F., Helman, M.L., Knott, S.D., Turco, E., Hutton, D.H.W., 1989. Kinematics of the western
765   Mediterranean. Geological Society, London, Special Publications 45, 265–283.
766   https://doi.org/10.1144/gsl.sp.1989.045.01.15
767 Diaz, J., Gallart, J., Carbonell, R., 2016. Moho topography beneath the Iberian-Western Mediterranean region
768   mapped from controlled-source and natural seismicity surveys. Tectonophysics 692, 74–85.
769   https://doi.org/10.1016/j.tecto.2016.08.023
770 Do Couto, D., Gumiaux, C., Augier, R., Lebret, N., Folcher, N., Jouannic, G., Jolivet, L., Suc, J., Gorini, C., 2014.
771   Tectonic inversion of an asymmetric graben: Insights from a combined field and gravity survey in the Sorbas
772   basin. Tectonics 33, 1360–1385. https://doi.org/10.1002/2013tc003458
773 Duggen, S., Hoernle, K., Bogaard, P. van den, Rüpke, L., Morgan, J.P., 2003. Deep roots of the Messinian salinity
774   crisis. Nature 422, 602–606. https://doi.org/10.1038/nature01553
775 Duggen, S., Hoernle, K., Bogaard, P. van den, Harris, C., 2004. Magmatic evolution of the Alboran region: The role
776   of subduction in forming the western Mediterranean and causing the Messinian Salinity Crisis. Earth Planet Sc
777   Lett 218, 91–108. https://doi.org/10.1016/s0012-821x(03)00632-0
778 Duggen, S., Hoernle, K., Klügel, A., Geldmacher, J., Thirlwall, M., Hauff, F., Lowry, D., Oates, N., 2008.
779   Geochemical zonation of the Miocene Alborán Basin volcanism (westernmost Mediterranean): geodynamic
780   implications. Contrib Mineral Petr 156, 577. https://doi.org/10.1007/s00410-008-0302-4
781 Echeverria, A., Khazaradze, G., Asensio, E., Gárate, J., Dávila, J.M., Suriñach, E., 2013. Crustal deformation in
782   eastern Betics from CuaTeNeo GPS network. Tectonophysics 608, 600–612.
783   https://doi.org/10.1016/j.tecto.2013.08.020
784 Ercilla, G., Galindo-Zaldívar, J., Estrada, F., Valencia, J., Juan, C., Casas, D., Alonso, B., Comas, M.C., Tendero-
785   Salmerón, V., Casalbore, D., Azpiroz-Zabala, M., Bárcenas, P., Ceramicola, S., Chiocci, F.L., Idárraga-García,
786   J., López-González, N., Mata, P., Palomino, D., Rodríguez-García, J.A., Teixeira, M., Nespereira, J., Vázquez,
787   J.T., Yenes, M., 2022. Understanding the complex geomorphology of a deep sea area affected by continental
788   tectonic indentation: The case of the Gulf of Vera (Western Mediterranean). Geomorphology 402, 108126.
789   https://doi.org/10.1016/j.geomorph.2022.108126

790 Faccenna, C., Becker, T.W., Auer, L., Billi, A., Boschi, L., Brun, J.P., Capitanio, F.A., Funiciello, F., Horvàth, F.,
791   Jolivet, L., Piromallo, C., Royden, L., Rossetti, F., Serpelloni, E., 2014. Mantle dynamics in the Mediterranean.
792   Rev Geophys 52, 283–332. https://doi.org/10.1002/2013rg000444

793 Fortuin, A.R., Krijgsman, W., 2003. The Messinian of the Nijar Basin (SE Spain): sedimentation, depositional
794   environments and paleogeographic evolution. Sediment Geol 160, 213–242. https://doi.org/10.1016/s0037-
795   0738(02)00377-9

796 Fossen, H., Teyssier, C., Whitney, D.L., 2013. Transtensional folding. Journal of structural geology 56, 89–102.
797   https://doi.org/http://dx.doi.org/10.1016/j.jsg.2013.09.004

798 Fossen, H., Tikoff, B., 1998. Extended models of transpression and transtension, and application to tectonic settings.
799   Geological Society, London, Special Publications 135, 15–33. https://doi.org/10.1144/gsl.sp.1998.135.01.02

800 Galindo-Zaldivar, J., Gonzalez-Lodeiro, F., Jabaloy, A., 2015. Progressive extensional shear structures in a
801   detachment contact in the Western Sierra Nevada (Betic Cordilleras, Spain). Geodin Acta 3, 73–85.
802   https://doi.org/10.1080/09853111.1989.11105175

803 Galindo-Zaldivar, J., Gil, A.J., Borque, M.J., González-Lodeiro, F., Jabaloy, A., Marin-Lechado, C., Ruano, P.,
804   Galdeano, C.S. de, 2003. Active faulting in the internal zones of the central Betic Cordilleras (SE, Spain). J
805   Geodyn 36, 239–250. https://doi.org/10.1016/s0264-3707(03)00049-8

806 Gallais, F., Graindorge, D., Gutscher, M.-A., Klaeschen, D., 2013. Propagation of a lithospheric tear fault (STEP)
807   through the western boundary of the Calabrian accretionary wedge offshore eastern Sicily (Southern Italy).
808   Tectonophysics 602, 141–152. https://doi.org/10.1016/j.tecto.2012.12.026

809 Garcia-Castellanos, D., Villaseñor, A., 2012. Messinian salinity crisis regulated by competing tectonics and erosion
810   at the Gibraltar arc. Nature 480, 359–363. https://doi.org/10.1038/nature10651

811 García-Dueñas, V., Banda, E., Torné, M., Córdoba, D., Group, E.-B.W., 1994. A deep seismic reflection survey
812   across the Betic Chain (southern Spain): first results. Tectonophysics 232, 77–89. https://doi.org/10.1016/0040-
813   1951(94)90077-9

814 Giaconia, F., Booth-Rea, G., Martínez-Martínez, J.M., Azañón, J.M., Pérez-Peña, J.V., Pérez-Romero, J., Villegas,
815   I., 2012. Geomorphic evidence of active tectonics in the Sierra Alhamilla (eastern Betics, SE Spain).
816   Geomorphology 145, 90–106. https://doi.org/10.1016/j.geomorph.2011.12.043

817 Giaconia, F., Booth-Rea, G., Martínez-Martínez, J.M., Azañón, J.M., Pérez-Romero, J., Villegas, I., 2013. Mountain
818   front migration and drainage captures related to fault segment linkage and growth: The Polopos transpressive
819   fault zone (southeastern Betics, SE Spain). J Struct Geol 46, 76–91. https://doi.org/10.1016/j.jsg.2012.10.005

820 Giaconia, F., Booth-Rea, G., Martinez-Martinez, J.M., Azañón, J.M., Storti, F., Artoni, A., 2014. Heterogeneous
821   extension and the role of transfer faults in the development of the southeastern Betic basins (SE Spain).
822   Tectonics 33, 2467–2489. https://doi.org/10.1002/2014tc003681

823 Giaconia, F., Booth-Rea, G., Ranero, C.R., Gràcia, E., Bartolome, R., Calahorrano, A., Iacono, C.L., Vendrell,
824   M.G., Cameselle, A.L., Costa, S., Peña, L.G. de la, Martínez-Loriente, S., Perea, H., Viñas, M., 2015.
825   Compressional tectonic inversion of the Algero-Balearic basin: Latemost Miocene to present oblique
826   convergence at the Palomares margin (Western Mediterranean): Tectonic Inversion of Palomares Margin.
827   Tectonics 34, 1516–1543. https://doi.org/10.1002/2015tc003861

828 Gomez-Pugnaire, M.T., Fernandez-Soler, J.M., 1987. High-pressure metamorphism in metabasites from the Betic
829   Cordilleras (S.E. Spain) and its evolution during the Alpine orogeny. Contrib Mineral Petr 95, 231–244.
830   https://doi.org/10.1007/bf00381273

831 Gómez de la Peña, L.G. de la, Grevemeyer, I., Kopp, H., Díaz, J., Gallart, J., Booth-Rea, G., Gràcia, E., Ranero,
832   C.R., 2020a. The Lithospheric Structure of the Gibraltar Arc System From Wide-Angle Seismic Data. J Geophys
833   Res Solid Earth 125. https://doi.org/10.1029/2020jb019854

834 Gómez de la Peña, L.G. de la, Ranero, C.R., Gràcia, E., 2018. The Crustal Domains of the Alboran Basin (Western
835   Mediterranean). Tectonics 37, 3352–3377. https://doi.org/10.1029/2017tc004946

836 Gómez de la Peña, L.G. de la, Ranero, C.R., Gràcia, E., Booth-Rea, G., 2020b. The evolution of the westernmost
837   Mediterranean basins. Earth-sci Rev 103445. https://doi.org/10.1016/j.earscirev.2020.103445

838 Govers, R., Wortel, M.J.R., 2005. Lithosphere tearing at STEP faults: response to edges of subduction zones. Earth
839   Planet Sc Lett 236, 505–523. https://doi.org/10.1016/j.epsl.2005.03.022

840 Haq, B., Gorini, C., Baur, J., Moneron, J., & Rubino, J.-L. (2020). Deep Mediterranean's Messinian evaporite giant:
841   How much salt? Global and Planetary Change, 184, 103052.
842   doi:https://doi.org/10.1016/j.gloplacha.2019.103052

843 Haughton, P.D.W., 2000. Evolving turbidite systems on a deforming basin floor, Tabernas, SE Spain.
844   Sedimentology 47, 497–518. https://doi.org/10.1046/j.1365-3091.2000.00293.x

845 Haughton, P.D.W., 1994. Deposits of deflected and ponded turbidity currents, Sorbas Basin, Southeast Spain. J
846   Sediment Res 64, 233–246. https://doi.org/10.1306/d4267d6b-2b26-11d7-8648000102c1865d
847 Heit, B., Mancilla, F. de L., Yuan, X., Morales, J., Stich, D., Martín, R., Molina-Aguilera, A., 2017. Tearing of the
848   mantle lithosphere along the intermediate-depth seismicity zone beneath the Gibraltar Arc: The onset of
849   lithospheric delamination. Geophys Res Lett 44, 4027–4035. https://doi.org/10.1002/2017gl073358
850 Hodgson, D.M., Haughton, P.D.W., 2004. Impact of syndepositional faulting on gravity current behaviour and deep-
851   water stratigraphy: Tabernas-Sorbas Basin, SE Spain. Geological Soc Lond Special Publ 222, 135–158.
852   https://doi.org/10.1144/gsl.sp.2004.222.01.08
853 Jabaloy-Sánchez, A., Talavera, C., Rodríguez-Peces, M.J., Vázquez-Vílchez, M., Evans, N.J., 2021. U-Pb
854   geochronology of detrital and igneous zircon grains from the Águilas Arc in the Internal Betics (SE Spain):
855   Implications for Carboniferous-Permian paleogeography of Pangea. Gondwana Res 90, 135–158.
856   https://doi.org/10.1016/j.gr.2020.10.013
857 Janowski, M., Loget, N., Gautheron, C., Barbarand, J., Bellahsen, N., Driessche, J.V. den, Babault, J., Meyer, B.,
858   2017. Neogene exhumation and relief evolution in the eastern Betics (SE Spain): Insights from the Sierra de
859   Gador. Terra Nova 29, 91–97. https://doi.org/10.1111/ter.12252
860 Johnson, C., Harbury, N., Hurford, A.J., 1997. The role of extension in the Miocene denudation of the Nevado-
861   Filábride Complex, Betic Cordillera (SE Spain). Tectonics 16, 189–204. https://doi.org/10.1029/96tc03289
862 Jolivet, L., Baudin, T., Calassou, S., Chevrot, S., Ford, M., Issautier, B., Lasseur, E., Masini, E., Manatschal, G.,
863   Mouthereau, F., Thinon, I., Vidal, O., 2021a. Geodynamic evolution of a wide plate boundary in the Western
864   Mediterranean, near-field versus far-field interactions. Bsgf - Earth Sci Bulletin 192, 48.
865   https://doi.org/10.1051/bsgf/2021043
866 Jolivet, L., Faccenna, C., 2000. Mediterranean extension and the Africa-Eurasia collision. Tectonics 19, 1095–1106.
867   https://doi.org/10.1029/2000tc900018
868 Jolivet, L., Menant, A., Roche, V., Le Pourhiet, L., Maillard, A., Augier, R., Couto, D.D., Gorini, C., Thinon, I.,
869   Canva, A., 2021b. Transfer zones in Mediterranean back-arc regions and tear faults. Bsgf - Earth Sci Bulletin
870   192, 11. https://doi.org/10.1051/bsgf/2021006
871 Jourdon, A., Kergaravat, C., Duclaux, G., Huguen, C., 2021. Looking beyond kinematics: 3D thermo-mechanical
872   modelling reveals the dynamics of transform margins. Solid Earth 12, 1211–1232. https://doi.org/10.5194/se-12-
873   1211-2021
874 Juan, C., Ercilla, G., Javier Hernández-Molina, F., Estrada, F., Alonso, B., Casas, D., . . . Ammar, A. (2016).
875   Seismic evidence of current-controlled sedimentation in the Alboran Sea during the Pliocene and Quaternary:
876   Palaeoceanographic implications. Marine Geology, 378, 292-311.
877   doi:https://doi.org/10.1016/j.margeo.2016.01.006
878 Jurado, M.J., Comas, M.C., 1992. Well log interpretation and seismic character of the cenozoic sequence in the
879   northern Alboran Sea. Geo-Marine Letters 12, 129–136.
880 Kleverlaan, K., 1989. Neogene history of the Tabernas basin (SE Spain) and its Tortonian submarine fan
881   development. Geologie en Mijnbouw 421–432.
882 Kleverlaan, K., 1989. Three distinctive feeder-lobe systems within one time slice of the Tortonian Tabernas fan, SE
883   Spain. Sedimentology 36, 25–45. https://doi.org/10.1111/j.1365-3091.1989.tb00818.x
884 Kleverlaan, K., 1987. Gordo megabed: a possible seismite in a tortonian submarine fan, tabernas basin, province
885   almeria, southeast spain. Sediment Geol 51, 165–180. https://doi.org/10.1016/0037-0738(87)90047-9
886 Koulali, A., Ouazar, D., Tahayt, A., King, R.W., Vernant, P., Reilinger, R.E., McClusky, S., Mourabit, T., Davila,
887   J.M., Amraoui, N., 2011. New GPS constraints on active deformation along the Africa–Iberia plate boundary.
888   Earth Planet Sc Lett 308, 211–217. https://doi.org/10.1016/j.epsl.2011.05.048
889 Larouzière, F.D.D., Bolze, J., Bordet, P., Hernandez, J., Montenat, C., d'Estevou, P.O., 1988. The Betic segment of
890   the lithospheric Trans-Alboran shear zone during the Late Miocene. Tectonophysics 152, 41–52.
891   https://doi.org/10.1016/0040-1951(88)90028-5
892 Le Pourhiet, L., Huet, B., May, D.A., Labrousse, L., Jolivet, L., 2012. Kinematic interpretation of the 3D shapes of
893   metamorphic core complexes: 3D SHAPES OF MCCs. Geochem Geophys Geosystems 13.
894   https://doi.org/10.1029/2012gc004271.
895 Lonergan, L., White, N., 1997. Origin of the Betic-Rif mountain belt. Tectonics 16, 504–522.
896   https://doi.org/10.1029/96tc03937
897 Mancilla, F. de L., Booth-Rea, G., Stich, D., Pérez-Peña, J.V., Morales, J., Azañón, J.M., Martin, R., Giaconia, F.,
898   2015a. Slab rupture and delamination under the Betics and Rif constrained from receiver functions.
899   Tectonophysics. https://doi.org/10.1016/j.tecto.2015.06.028

Mancilla, F. de L., Heit, B., Morales, J., Yuan, X., Stich, D., Molina-Aguilera, A., Azañon, J.M., Martín, R., 2018. A STEP fault in Central Betics, associated with lateral lithospheric tearing at the northern edge of the Gibraltar arc subduction system. Earth Planet Sc Lett 486, 32–40. https://doi.org/10.1016/j.epsl.2018.01.008

Mancilla, F. de L., Stich, D., Morales, J., Martin, R., Diaz, J., Pazos, A., Córdoba, D., Pulgar, J.A., Ibarra, P., Harnafi, M., Gonzalez-Lodeiro, F., 2015b. Crustal thickness and images of the lithospheric discontinuities in the Gibraltar arc and surrounding areas. Geophysical Journal International 203, 1804–1820. https://doi.org/10.1093/gji/ggv390

Martin, J.M., Braga, J.C., Rivas, P., 1989. Coral successions in Upper Tortonian reefs in SE Spain. Lethaia 22, 271–286. https://doi.org/10.1111/j.1502-3931.1989.tb01342.x

Martín, J.M., Braga, J.C., 1994. Messinian events in the Sorbas Basin in southeastern Spain and their implications in the recent history of the Mediterranean. Sediment Geol 90, 257–268. https://doi.org/10.1016/0037-0738(94)90042-6

Martínez-García, P., Comas, M., Lonergan, L., Watts, A.B., 2017. From Extension to Shortening: Tectonic Inversion Distributed in Time and Space in the Alboran Sea, Western Mediterranean. Tectonics 36, 2777–2805. https://doi.org/10.1002/2017tc004489

Martínez-García, P., Soto, J.I., Comas, M., 2011. Recent structures in the Alboran Ridge and Yusuf fault zones based on swath bathymetry and sub-bottom profiling: evidence of active tectonics. Geo-mar Lett 31, 19–36. https://doi.org/10.1007/s00367-010-0212-0

Martínez-Martínez, J.M., Azañón, J.M., 1997. Mode of extensional tectonics in the southeastern Betics (SE Spain): Implications for the tectonic evolution of the peri-Alborán orogenic system. Tectonics 16, 205–225. https://doi.org/10.1029/97tc00157

Martínez-Martínez, J.M., Booth-Rea, G., Azañón, J.M., Torcal, F., 2006. Active transfer fault zone linking a segmented extensional system (Betics, southern Spain): Insight into heterogeneous extension driven by edge delamination. Tectonophysics 422, 159–173. https://doi.org/10.1016/j.tecto.2006.06.001

Martínez-Martínez, J.M., Soto, J.I., Balanyá, J.C., 2002. Orthogonal folding of extensional detachments: Structure and origin of the Sierra Nevada elongated dome (Betics, SE Spain). Tectonics 21, 3-1-3–20. https://doi.org/10.1029/2001tc001283

Martinez-Martínez, J.M., Soto, J.I., Balanyá, J.C., 2004. Elongated domes in extended orogens: A mode of mountain uplift in the Betics (southeast Spain), in: Special Paper 380: Gneiss Domes in Orogeny. Geological Society of America, pp. 243–265. https://doi.org/10.1130/0-8137-2380-9.243

Martínez-Martos, M., Galindo-Zaldivar, J., Martínez-Moreno, F.J., Calvo-Rayo, R., Galdeano, C.S. de, 2017. Superposition of tectonic structures leading elongated intramontane basin: the Alhabia basin (Internal Zones, Betic Cordillera). Int J Earth Sci 106, 2461–2471. https://doi.org/10.1007/s00531-016-1442-9

Meighan, H.E., Brink, U. ten, Pulliam, J., 2013. Slab tears and intermediate-depth seismicity: slab tears and intermediate seismicity. Geophys Res Lett 40, 4244–4248. https://doi.org/10.1002/grl.50830

Meijninger, B.M.L., Vissers, R.L.M., 2006. Miocene extensional basin development in the Betic Cordillera, SE Spain revealed through analysis of the Alhama de Murcia and Crevillente Faults: Miocene extensional basin development in the Betic Cordillera. Basin Res 18, 547–571. https://doi.org/10.1111/j.1365-2117.2006.00308.x

Montenat, C., D'Estevou, P.O., 1992. Geodynamics of the Eastern Betic late Neogene Basins. A Review. Física de la Tierra 57–75.

Montenat, C., d'Estevou, P.O., 1999. The diversity of late Neogene sedimentary basins generated by wrench faulting in the eastern Betic Cordillera, SE Spain. J Petrol Geol 22, 61–80. https://doi.org/10.1111/j.1747-5457.1999.tb00459.x

Mora, M., 1993. Tectonic and sedimentary analysis of the Huercal-Overa region, South East Spain, Betic Cordillera. University of Oxford, 300 pp.

Moragues, L., Ruano, P., Azañón, J.M., Garrido, C.J., Hidas, K., Booth-Rea, G., 2021. Two Cenozoic Extensional Phases in Mallorca and Their Bearing on the Geodynamic Evolution of the Western Mediterranean. Tectonics 40. https://doi.org/10.1029/2021tc006868.

Mouthereau, F., Angrand, P., Jourdon, A., Ternois, S., Fillon, C., Calassou, S., Chevrot, S., Ford, M., Jolivet, L., Manatschal, G., Masini, E., Thinon, I., Vidal, O., Baudin, T., 2021. Cenozoic mountain building and topographic evolution in Western Europe: impact of billions of years of lithosphere evolution and plate kinematics. Bsgf - Earth Sci Bulletin 192, 56. https://doi.org/10.1051/bsgf/2021040

Mouthereau, F., Filleaudeau, P., Vacherat, A., Pik, R., Lacombe, O., Fellin, M.G., Castelltort, S., Christophoul, F., Masini, E., 2014. Placing limits to shortening evolution in the Pyrenees: Role of margin architecture and implications for the Iberia/Europe convergence. Tectonics 33, 2283–2314. https://doi.org/10.1002/2014tc003663

955 Neuharth, D., Brune, S., Glerum, A., Morley, C.K., Yuan, X., Braun, J., 2021. Flexural strike-slip basins. Geology.
956   https://doi.org/10.1130/g49351.1
957 Nocquet, J.-M., 2012. Present-day kinematics of the Mediterranean: A comprehensive overview of GPS results.
958   Tectonophysics 579, 220–242. https://doi.org/10.1016/j.tecto.2012.03.037
959 Okay, A.I., Tüysüz, O., Kaya, Ş., 2004. From transpression to transtension: changes in morphology and structure
960   around a bend on the North Anatolian Fault in the Marmara region. Tectonophysics 391, 259–282.
961   https://doi.org/10.1016/j.tecto.2004.07.016
962 Palano, M., González, P.J., Fernández, J., 2015. The Diffuse Plate boundary of Nubia and Iberia in the Western
963   Mediterranean: Crustal deformation evidence for viscous coupling and fragmented lithosphere. Earth and
964   Planetary Science Letters 430, 439–447. https://doi.org/10.1016/j.epsl.2015.08.040
965 Palano, M., González, P.J., Fernández, J., 2013. Strain and stress fields along the Gibraltar Orogenic Arc:
966   Constraints on active geodynamics. Gondwana Res 23, 1071–1088. https://doi.org/10.1016/j.gr.2012.05.021
967 Palomeras, I., Thurner, S., Levander, A., Liu, K., Villaseñor, A., Carbonell, R., Harnafi, M., 2014. Finite-frequency
968   Rayleigh wave tomography of the western Mediterranean: Mapping its lithospheric structure. Geochemistry,
969   Geophysics, Geosystems 15, 140–160. https://doi.org/10.1002/2013gc004861
970 Pedrera, A., Galindo-Zaldívar, J., Galdeano, C.S. de, López-Garrido, Á.C., 2007. Fold and fault interactions during
971   the development of an elongated narrow basin: The Almanzora Neogene-Quaternary Corridor (SE Betic
972   Cordillera, Spain): FOLD AND FAULT INTERACTIONS. Tectonics 26, n/a-n/a.
973   https://doi.org/10.1029/2007tc002138
974 Pedrera, A., Galindo-Zaldívar, J., Ruíz-Constán, A., Duque, C., Marín-Lechado, C., Serrano, I., 2009. Recent large
975   fold nucleation in the upper crust: Insight from gravity, magnetic, magnetotelluric and seismicity data (Sierra de
976   Los Filabres–Sierra de Las Estancias, Internal Zones, Betic Cordillera). Tectonophysics 463, 145–160.
977   https://doi.org/10.1016/j.tecto.2008.09.037
978 Pedrera, A., Galindo-Zaldívar, J., Tello, A., Marín-Lechado, C., 2010. Intramontane basin development related to
979   contractional and extensional structure interaction at the termination of a major sinistral fault: The Huércal-
980   Overa Basin (Eastern Betic Cordillera). J Geodyn 49, 271–286. https://doi.org/10.1016/j.jog.2010.01.008
981 Pickering, K.T., Hodgson, D.M., Platzman, E., Clark, J.D., Stephens, C., 2001. A New Type of Bedform Produced
982   by Backfilling Processes in a Submarine Channel, Late Miocene, Tabernas-Sorbas Basin, SE Spain. J Sediment
983   Res 71, 692–704. https://doi.org/10.1306/2dc40960-0e47-11d7-8643000102c1865d
984 Pindell, J.L., Kennan, L., 2009. Tectonic evolution of the Gulf of Mexico, Caribbean and northern South America in
985   the mantle reference frame: an update. Geological Soc Lond Special Publ 328, 1–55.
986   https://doi.org/10.1144/sp328.1
987 Platt, J.P., Behr, W.M., Johanesen, K., Williams, J.R., 2013. The Betic-Rif Arc and Its Orogenic Hinterland: A
988   Review. Annual Review of Earth and Planetary Sciences 41, 313–357. https://doi.org/10.1146/annurev-earth-
989   050212-123951
990 Platt, J.P., Kelley, S.P., Carter, A., Orozco, M., 2005. Timing of tectonic events in the Alpujárride Complex, Betic
991   Cordillera, southern Spain. J Geol Soc London 162, 451–462. https://doi.org/10.1144/0016-764903-039
992 Platt, J.P., Whitehouse, M.J., Kelley, S.P., Carter, A., Hollick, L., 2003. Simultaneous extensional exhumation
993   across the Alboran Basin: Implications for the causes of late orogenic extension. Geology 31, 251–254.
994   https://doi.org/10.1130/0091-7613(2003)031<0251:seeata>2.0.co;2
995 Platt, J.P., Anczkiewicz, R., Soto, J.-I., Kelley, S.P., Thirlwall, M., 2006. Early Miocene continental subduction and
996   rapid exhumation in the western Mediterranean. Geology 34, 981–984. https://doi.org/10.1130/g22801a.1
997 Platt, J.P., Vissers, R.L.M., 1989. Extensional collapse of thickened continental lithosphere: A working hypothesis
998   for the Alboran Sea and Gibraltar arc. Geology 17, 540–543. https://doi.org/10.1130/0091-
999   7613(1989)017<0540:ecotcl>2.3.co;2
1000 Platt, J.P., Whitehouse, M.J., 1999. Early Miocene high-temperature metamorphism and rapid exhumation in the
1001   Betic Cordillera (Spain): evidence from U–Pb zircon ages. Earth and Planetary Science Letters 171, 591–605.
1002 Platzman, E.S., 1992. Paleomagnetic rotations and the kinematics of the Gibraltar arc. Geology 20, 311–314.
1003   https://doi.org/10.1130/0091-7613(1992)020<0311:pratko>2.3.co;2
1004 Poisson, A., Guezou, J.C., Ozturk, A., Inan, S., Temiz, H., Gürsöy, H., Kavak, K.S., ÖZDEN, S., 1996. Tectonic
1005   Setting and Evolution of the Sivas Basin, Central Anatolia, Turkey. International Geology Review 38, 838–853.
1006   https://doi.org/10.1080/00206819709465366
1007 Poisson, A.M., Morel, J.L., Andrieux, J., Coulon, M., Wernli, R., Guernet, C., 1999. The origin and development of
1008   neogene basins in the SE Betic Cordillera (SE Spain): a case study of the Tabernas-Sorbas and Huercal Overa
1009   basins. J Petrol Geol 22, 97–114. https://doi.org/10.1111/j.1747-5457.1999.tb00461.x

1010 Pownall, J.M., Hall, R., Watkinson, I.M., 2013. Extreme extension across Seram and Ambon, eastern Indonesia:
1011   evidence for Banda slab rollback. Solid Earth 4, 277–314. https://doi.org/10.5194/se-4-277-2013
1012 Rat, J., Mouthereau, F., Brichau, S., Crémades, A., Bernet, M., Balvay, M., Ganne, J., Lahfid, A., Gautheron, C.,
1013   2019. Tectonothermal Evolution of the Cameros Basin: Implications for Tectonics of North Iberia. Tectonics 38,
1014   440–469. https://doi.org/10.1029/2018tc005294
1015 Rat, J., Mouthereau, F., Brichau, S., Vacherat, A., Fillon, C., Gautheron, C., 2022. Timing and distribution of
1016   exhumation in the Ebro basin reveal a plate-scale 10 Ma geodynamic event. Global Planet Change 103973.
1017   https://doi.org/10.1016/j.gloplacha.2022.103973
1018 Reicherter, K., Hübscher, C., 2006. Evidence for a seafloor rupture of the Carboneras Fault Zone (southern Spain):
1019   Relation to the 1522 Almería earthquake? J Seismol 11, 15–26. https://doi.org/10.1007/s10950-006-9024-0
1020 Reinhardt, L.J., Dempster, T.J., Shroder, J.F., Persano, C., 2007. Tectonic denudation and topographic development
1021   in the Spanish Sierra Nevada. Tectonics 26, n/a-n/a. https://doi.org/10.1029/2006tc001954
1022 Richards, J.P., 2009. Postsubduction porphyry Cu-Au and epithermal Au deposits: Products of remelting of
1023   subduction-modified lithosphere. Geology 37, 247–250. https://doi.org/10.1130/g25451a.1
1024 Riding, R., Braga, J.C., Martín, J.M., Sánchez-Almazo, I.M., 1998. Mediterranean Messinian Salinity Crisis:
1025   constraints from a coeval marginal basin, Sorbas, southeastern Spain. Mar Geol 146, 1–20.
1026   https://doi.org/10.1016/s0025-3227(97)00136-9
1027 Rodríguez-Fernández, J., Azor, A., Azañón, J.M., 2012. Tectonics of Sedimentary Basins 461–479.
1028   https://doi.org/10.1002/9781444347166.ch23
1029 Romagny, A., Jolivet, L., Menant, A., Bessière, E., Maillard, A., Canva, A., Gorini, C., Augier, R., 2020. Detailed
1030   tectonic reconstructions of the Western Mediterranean region for the last 35 Ma, insights on driving
1031   mechanisms. Bsgf - Earth Sci Bulletin 191, 37. https://doi.org/10.1051/bsgf/2020040
1032 Rosenbaum, G., Lister, G.S., Duboz, C., 2002. Relative motions of Africa, Iberia and Europe during Alpine
1033   orogeny. Tectonophysics 359, 117–129. https://doi.org/10.1016/s0040-1951(02)00442-0
1034 Sanz de Galdeano, C.S., Vera, J.A., 1992. Stratigraphic record and palaeogeographical context of the Neogene
1035   basins in the Betic Cordillera, Spain. Basin Res 4, 21–36. https://doi.org/10.1111/j.1365-2117.1992.tb00040.x
1036 Sanz de Galdeano, C.S.D., Rodriguez-Fernandez, J., Lopez-Garrido, A.C., 1985. A strike-slip fault corridor within
1037   the Alpujarra Mountains (Betic Cordilleras, Spain). Geol Rundsch 74, 641–655.
1038   https://doi.org/10.1007/bf01821218
1039 Sanz de Galdeano, C.S. de, Alfaro, P., 2004. Tectonic significance of the present relief of the Betic Cordillera.
1040   Geomorphology 63, 175–190. https://doi.org/10.1016/j.geomorph.2004.04.002
1041 Scotney, P., Burgess, R., Rutter, E.H., 2000. 40Ar/39Ar age of the Cabo de Gata volcanic series and displacements
1042   on the Carboneras fault zone, SE Spain. J Geol Soc London 157, 1003–1008.
1043   https://doi.org/10.1144/jgs.157.5.1003
1044 Sosson, M., Morrillon, A.-C., Bourgois, J., Féraud, G., Poupeau, G., Saint-Marc, P., 1998. Late exhumation stages
1045   of the Alpujarride Complex (western Betic Cordilleras, Spain): new thermochronological and structural data on
1046   Los Reales and Ojen nappes. Tectonophysics 285, 253–273. https://doi.org/10.1016/s0040-1951(97)00274-6
1047 Spakman, W., Wortel, R., 2004. The TRANSMED Atlas. The Mediterranean Region from Crust to Mantle 31–52.
1048   https://doi.org/10.1007/978-3-642-18919-7_2
1049 Spakman, W., Chertova, M.V., Berg, A. van Hinsbergen, D.J.J., 2018. Puzzling features of western Mediterranean
1050   tectonics explained by slab dragging. Nat Geosci 11. https://doi.org/10.1038/s41561-018-0066-z
1051 Stich, D., Serpelloni, E., Mancilla, F. de L., Morales, J., 2006. Kinematics of the Iberia–Maghreb plate contact from
1052   seismic moment tensors and GPS observations. Tectonophysics 426, 295–317.
1053   https://doi.org/10.1016/j.tecto.2006.08.004
1054 Tendero-Salmerón, V., Galindo-Zaldívar, J., d'Acremont, E., Catalán, M., Martos, Y.M., Ammar, A., Ercilla, G.,
1055   2022. New insights on the Alboran Sea basin extension and continental collision from magnetic anomalies
1056   related to magmatism (western Mediterranean). Mar Geol 443, 106696.
1057   https://doi.org/10.1016/j.margeo.2021.106696
1058 Teyssier, C., Tikoff, B., 1998. Strike-slip partitioned transpression of the San Andreas fault system: a lithospheric-
1059   scale approach. Geological Soc Lond Special Publ 135, 143–158. https://doi.org/10.1144/gsl.sp.1998.135.01.10
1060 Vacherat, A., Mouthereau, F., Pik, R., Bellahsen, N., Gautheron, C., Bernet, M., Daudet, M., Balansa, J., Tibari, B.,
1061   Jamme, R.P., Radal, J., 2016. Rift-to-collision transition recorded by tectonothermal evolution of the northern
1062   Pyrenees. Tectonics 35, 907–933. https://doi.org/10.1002/2015tc004016
1063 van Hinsbergen, D.J.J., Vissers, R.L.M., Spakman, W., 2014. Origin and consequences of western Mediterranean
1064   subduction, rollback, and slab segmentation. Tectonics 33, 393–419. https://doi.org/10.1002/2013tc003349

1065 Vázquez, M., Jabaloy, A., Barbero, L., Stuart, F.M., 2011. Deciphering tectonic- and erosion-driven exhumation of
1066   the Nevado-Filábride Complex (Betic Cordillera, Southern Spain) by low temperature thermochronology:
1067   Deciphering tectonic- and erosion-driven exhumation. Terra Nova 23, 257–263. https://doi.org/10.1111/j.1365-
1068   3121.2011.01007.x
1069 Vergés, J., Fernàndez, M., 2012. Tethys–Atlantic interaction along the Iberia–Africa plate boundary: The Betic–Rif
1070   orogenic system. Tectonophysics 579, 144–172. https://doi.org/10.1016/j.tecto.2012.08.032
1071 Vernant, P., Fadil, A., Mourabit, T., Ouazar, D., Koulali, A., Davila, J.M., Garate, J., McClusky, S., Reilinger, R.,
1072   2010. Geodetic constraints on active tectonics of the Western Mediterranean: Implications for the kinematics and
1073   dynamics of the Nubia-Eurasia plate boundary zone. J Geodyn 49, 123–129.
1074   https://doi.org/10.1016/j.jog.2009.10.007
1075 Villasenor, A., Chevrot, S., Harnafi, M., Gallart, J., Pazos, A., Serrano, I., Córdoba, D., Pulgar, J.A., Ibarra, P.,
1076   2015. Subduction and volcanism in the Iberia–North Africa collision zone from tomographic images of the
1077   upper mantle. Tectonophysics. https://doi.org/10.1016/j.tecto.2015.08.042
1078 Waldner, M., Bellahsen, N., Mouthereau, F., Bernet, M., Pik, R., Rosenberg, C.L., Balvay, M., 2021. Central
1079   Pyrenees Mountain Building: Constraints From New LT Thermochronological Data From the Axial Zone.
1080   Tectonics 40. https://doi.org/10.1029/2020tc006614
1081 Weijermars, R., Roep, Th.B., Eeckhout, B.V. den, Postma, G., Kleverlaan, K., 1985. Uplift history of a Betic fold
1082   nappe inferred from Neogene-Quaternary sedimentation and tectonics (in the Sierra Alhamilla and Almeria,
1083   Sorbas and Tabernas Basins of the Betic Cordilleras, SE Spain). Geologie en Mijnbouw 397–411.
1084 Zeck, H.P., Monié, P., Villa, I.M., Hansen, B.T., 1992. Very high rates of cooling and uplift in the Alpine belt of the
1085   Betic Cordilleras, southern Spain. Geology 20, 79. https://doi.org/10.1130/0091-
1086   7613(1992)020<0079:vhroca>2.3.co;2
1087